inhibition of phosphorylation of IκBα on Ser-32 by VEGF, IL-1β, and TNF-α. IKK exists as a high molecular complex containing two kinase subunits, IKKα (IKK1) and IKKβ (IKK2), and a regulatory subunit, NEMO [13]. The phosphorylation of IκBα on Ser-32 and Ser-36 is mediated mainly by the kinase activity of IKKβ and led to its proteolytic degradation and subsequent nuclear translocation of NF-κB [13]. Therefore, ERK is most likely to inhibit the canonical NF-κB pathway that involves IKK-mediated IκBα phosphorylation in endothelial cells.

In conclusion, our present data apparently demonstrate a novel function of ERK as a curb of endothelial NF-κB activation with possible mechanism (Fig. 8). Indeed, elevation of ERK activity in endothelial cells significantly suppressed expression of NF-κB-dependent genes such as ICAM-1 and VCAM-1 in response to cytokine stimulation. These effects were functionally correlated with decreased endothelial cell–monocyte interaction. Although the further study is required to prove the anti-inflammatory nature of ERK in more complex in vivo environment, our findings suggest that ERK activity constitutively or transiently induced by normal laminar flow or various endothelial stimuli may serve as a negative regulator of vascular inflammation by suppressing endothelial NF-κB activation. Therefore, measuring the existence of ERK activity in vascular endothelial cells may be useful for predicting the feasibility and potency of inflammatory reactions in the vascular wall.

Acknowledgments

This work was supported by a Next Generation Growth Engine Program Grant and Vascular System Research Center Grant from the Korean Ministry of Science and Technology.

References

[1] H. Ulbrich, E.E. Eriksson, L. Lindbom, Trends Pharmacol. Sci. 24 (2003) 640.
[2] D. Vestweber, Curr. Opin. Cell Biol. 14 (2002) 587.
[3] W.A. Muller, Lab Invest. 82 (2002) 521.
[4] P. Xia, J.R. Gamble, K.A. Rye, L. Wang, C.S. Hii, P. Cockerill, Y. Khew-Goodall, A.G. Bert, P.J. Barter, M.A. Vadas, Proc. Natl. Acad. Sci. U. S. A. 95 (1998) 14196.
[5] K.T. Piercy, R.L. Donnell, S.S. Kirkpatrick, C.H. Timaran, S.L. Stevens, M.B. Freeman, M.H. Goldman, J. Surg. Res. 105 (2002) 215.
[6] S. Zeuke, A.J. Ulmer, S. Kusumoto, H.A. Katus, H. Heine, Cardiovasc. Res. 56 (2002) 126.
[7] J. Peter, D.M. Barnes, Sc. D, Michael Karin, N. Engl. J. Med. 336 (1997) 1066.
[8] P.A. Baeuerle, T. Henkel, Annu. Rev. Immunol. 12 (1994) 141.
[9] C. Maaser, S. Schoeppner, T. Kucharzik, M. Kraft, E. Schoenherr, W. Domschke, N. Luegering, Clin. Exp. Immunol. 124 (2001) 208.
[10] J.T. Wu, J.G. Kral, J. Surg. Res. 123 (2005) 158.
[11] Y. Yamamoto, R.B. Gaynor, Trends Biochem. Sci. 29 (2004) 72.
[12] P. Viatour, M.P. Merville, V. Bours, A. Chariot, Trends Biochem Sci. 30 (2005) 43.
[13] M.S. Ayden, S. Hosh, Genes Dev. 18 (2004) 2195.
[14] E. Majewska, E. Paleolog, Z. Baj, U. Kralisz, M. Feldmann, H. Tchorzewski, Scand. J. Immunol. 45 (1997) 385.
[15] H. Zhang, A.C. Issekutz, Am. J. Pathol. 160 (2002) 2219.
[16] M. Kaneki, S. Kharbanda, P. Pandey, K. Yoshida, M. Takekawa, J.R. Liou, R. Stone, D. Kufe, Mol. Cell. Biol. 19 (1999) 461.
[17] R. Datta, K. Yoshinaga, M. Kaneki, P. Pandey, D. Kufe, J. Biol. Chem. 275 (2000) 41000.
[18] J.H. Je, J.Y. Lee, K.J. Jung, B. Sung, E.K. Go, B.P. Yu, H.Y. Chung, FEBS Lett. 566 (2004) 183.
[19] C. Schmidt, B. Peng, Z. Li, G.M. Sclabas, S. Fujioka, J. Niu, M. Schmidt-Supprian, D.B. Evans, J.L. Abbruzzese, P.J. Chiao, Mol. Cell. 12 (2003) 1287.
[20] J.R. Burke, J. Strnad, Biochem. Biophys. Res. Commun. 293 (2002) 1508.
[21] P.E. Hughes, M.W. Renshaw, M. Pfaff, J. Forsyth, V.M. Keivens, M.A. Schwartz, M.H. Ginsberg, Cell 88 (1997) 521.
[22] R. Gum, H. Wang, E. Lengyel, J. Juarez, D. Boyd, Oncogene 14 (1997) 481.
[23] D. Besser, M. Presta, Y. Nagamine, Cell Growth Differ. 6 (1995) 1009.
[24] E. Meylan, F. Martinon, M. Thome, M. Gschwendt, J. Tschopp, EMBO Rep. 3 (2002) 1201.
[25] E.A. Jaffe, R.L. Nachman, C.G. Becker, C.R. Minick, J. Clin. Invest. 52 (1973) 2745.
[26] T. Minami, W.C. Aird, J. Biol. Chem. 276 (2001) 47632.
[27] D. Cefai, E. Simeoni, K.M. Ludunge, R. Driscoll, L.K. von Segesser, L. Kappenberger, G. Vassalli, J. Mol. Cell. Cardiol. 38 (2005) 333.
[28] Y. Takada, A. Mukhopadhyay, G.C. Kundu, G.H. Mahabeleshwar, S. Singh, B.B. Aggarwal, J. Biol. Chem. 278 (2003) 24233.
[29] M.A. Proescholdt, S. Jacobson, N. Tresser, E.H. Oldfield, M.J. Merrill, J. Neuropathol. Exp. Neurol. 61 (2002) 914.
[30] S.D. Croll, J.H. Goodman, H.E. Scharfman, Adv. Exp. Med. Biol. 548 (2004) 57.
[31] I. Kim, S.O. Moon, S.H. Kim, H.J. Kim, Y.S. Koh, G.Y. Koh, J. Biol. Chem. 276 (2001) 7614.
[32] I. Kim, S.O. Moon, S.K. Park, S.W. Chae, G.Y. Koh, Circ. Res. 89 (2001) 477.
[33] H.J. Park, Y.W. Lee, B. Hennig, M. Toborek, Nutr. Cancer 41 (2001) 126.
[34] V. Dixit, T.W. Mak, Cell 111 (2002) 615.
[35] K. Page, J. Li, L. Zhou, S. Iasvovskaia, K.C. Corbit, J.W. Soh, I.B. Weinstein, A.R. Brasier, A. Lin, M.B. Hershenson, J. Immunol. 170 (2003) 5681.
[36] T. Minami, M.R. Abid, J. Zhang, G. King, T. Kodama, W.C. Aird, J. Biol. Chem. 278 (2003) 6976.
[37] G.P. Sorescu, M. Sykes, D. Weiss, M.O. Platt, A. Saha, J. Hwang, N. Boyd, Y.C. Boo, J.D. Vega, W.R. Taylor, H. Jo, J. Biol. Chem. 278 (2003) 31128.
[38] E. Eng, B.J. Ballermann, Microvasc. Res. 65 (2003) 137.
[39] B.H. Jeon, F. Khanday, S. Deshpande, A. Haile, M. Ozaki, K. Irani, Circ. Res. 92 (2003) 586.
[40] Y.M. Kim, Y.M. Kim, Y.M. Lee, H.S. Kim, J.D. Kim, Y. Choi, K.W. Kim, S.Y. Lee, Y.G. Kwon, J. Biol. Chem. 277 (2002) 6799.
[41] J.K. Min, Y.M. Kim, S.W. Kim, M.C. Kwon, Y.Y. Kong, I.K. Hwang, M. H. Won, J. Rho, Y.G. Kwon, J. Immunol. 175 (2005) 531.
[42] J.K. Min, Y.M. Lee, J.H. Kim, Y.M. Kim, S.W. Kim, S.Y. Lee, Y.S. Gho, G.T. Oh, Y.G. Kwon, Circ. Res. 96 (2005) 300.

Enhanced Functional Gap Junction Neoformation by Protein Kinase A–Dependent and Epac-Dependent Signals Downstream of cAMP in Cardiac Myocytes

Satoshi Somekawa, Shigetomo Fukuhara, Yoshikazu Nakaoka, Hisakazu Fujita, Yoshihiko Saito, Naoki Mochizuki

Abstract—Gap junctions (GJs) constituted by neighboring cardiac myocytes are essential for gating ions and small molecules to coordinate cardiac contractions. cAMP is suggested to be a potent stimulus for enhancement of GJ function. However, it remains elusive how cAMP potentiates the GJ of cardiomyocytes. Here we demonstrated that the gating function of GJ is enhanced by the protein kinase A (PKA)–dependent signal, and that the accumulation of connexin43 (Cx43), the most abundant Cx in myocytes, is enhanced by an exchange protein directly activated by cAMP (Epac) (Rap1 activator)–dependent signal. The gating function of GJs was analyzed by microinjected dye transfer method. The accumulation of Cx43 was analyzed by quantitative immunostaining. Using the PKA-specific activator N^6-benzoyladenosine-3′,5′-cyclic monophosphate (6Bnz) and Epac-specific activator 8-(4-chlorophenylthio)-2′-*O*-methyladenosine-3′,5′-cyclic monophosphate (8CPT), we could delineate the two important downstream signals of cAMP for enhanced GJ neoformation. Whereas 6Bnz potentiated gating function of GJs with slight accumulation of Cx43 at cell–cell contacts, 8CPT remarkably enhanced the accumulation of Cx43 with a slight effect on gating. We further noticed that adherens junctions (AJs) were maturated by 8CPT, as marked by increased neural-cadherin immunostaining. Because AJ formation precedes the GJ formation, AJ formation accelerated by Epac-Rap1 signal may result in enhanced GJ formation. The involvement of Epac-Rap1 signal in GJ neoformation was further confirmed by evidence that inactivation of Rap1 by overexpression of Rap1GAP1b perturbed the accumulation of Cx43 at cell–cell contacts. Collectively, PKA and Epac cooperatively enhance functional GJ neoformation in cardiomyocytes. (***Circ Res.* 2005;97:655-662.**)

Key Words: gap junction ■ connexin43 ■ myocardial structure ■ cardiac gap junction connexins

Gap junctions (GJs) are channels formed by two docking connexons; one connexon is provided by each of the two contiguous cells and is constituted of six connexin (Cx) molecules.[1] Among the 20 Cx members, Cx40, Cx43, and Cx45 are expressed in the heart.[2] Of the three, Cx43 is predominantly expressed in working heart muscle cells.[3,4] GJs in the heart are characterized by their localization at the intercalated disk between each myocyte and also by their role in electrical conductance required for coordinated electrical excitation.[5] Myocytes electrically coupled by GJs show synchronized contraction. The importance of Cx43 in electrical excitation in vivo is evident by cardiac-specific depletion of Cx43 leading to cardiac arrhythmia.[6]

The overall function of GJs depends on the number of GJs and the gating function of assembled GJs. GJs are upregulated by increased transcription of Cx, increased distribution of Cx at cell–cell contacts, and decreased degradation of Cx from the cell membrane. cAMP increases Cx43 mRNA.[7] cAMP also enhances the trafficking of Cx43 from the endoplasmic reticulum/Golgi apparatus to the plasma membrane.[8] Cx43 turnover is regulated by proteosomal and lysosomal degradation, and the half-life of Cx43 is less than two hours, suggesting that a rapid synthesis and trafficking system operates in cardiac myocytes.[9]

GJ is modulated by the phosphorylation of Cx43 on Ser and Tyr residues. The intercellular communication through Cx43 is decelerated and accelerated by its phosphorylation on Ser368 by protein kinase C and on Ser364 by protein kinase A (PKA), respectively.[10,11] In addition to Ser phosphorylation, phosphorylated Cx43 on Tyr247 and Tyr265 is repressed from junctional communication.[12] In addition to phosphorylation, GJ formation is regulated by Cx43-binding molecules. Cx43 binds to the junctional adhesion molecule-associating proteins zonula occludens-1 (ZO-1) and β-catenin.[13,14] Dominant-negative ZO-1, which dissociates the endogenous ZO-1 from Cx43, disturbs the localization of

Original received May 10, 2005; resubmission received July 12, 2005; revised resubmission received August 11, 2005; accepted August 16, 2005.

From the Department of Structural Analysis (S.F., Y.N., H.F., N.M.), National Cardiovascular Center Research Institute, Suita, Osaka; the First Department of Internal Medicine (S.S., Y.S.), Nara Medical University, Kashihara, Nara, Japan.

Correspondence to Naoki Mochizuki, Department of Structural Analysis, National Cardiovascular Center Research Institute, 5-7-1 Fujishirodai, Suita, Osaka 565-8565, Japan. E-mail nmochizu@ri.ncvc.go.jp

Circulation Research is available at http://circres.ahajournals.org DOI: 10.1161/01.RES.0000183880.49270.f9

Cx43 at the cell–cell contacts, resulting in the reduced conductance of GJs.[13] Wnt-1 signal prevents β-catenin degradation, thereby increasing β-catenin, which not only drives Cx43 expression but also associates with the Cx43 at the cell–cell contacts, where β-catenin localizes with cadherin.[14]

cAMP-induced Cx43 assembly has been extensively characterized in terms of Cx43 synthesis, delivery to the plasma membrane, and phosphorylation, which is believed to depend exclusively on PKA.[15] However, other downstream molecules of cAMP have not been elucidated in the neoformation of GJs. We and others have demonstrated that exchange protein directly activated by cAMP (Epac)/cAMP-GEF, a guanine nucleotide exchange factor (GEF) for Rap1, is activated by cAMP,[16,17] and that cAMP–Epac-Rap1 signal enhances the barrier function of vascular endothelial cells by stabilizing cadherin-mediated cell adhesion.[18,19] Analogous to this Epac-induced cadherin-based cell adhesion, we hypothesized that Epac may be involved in GJ neoformation as a cAMP-triggered signaling molecule in cardiac myocytes.

In this study, we investigated the molecular mechanism by which GJ neoformation is regulated by cAMP using a PKA-specific activator and an Epac-specific activator. We analyzed the GJ accumulation at cell–cell contacts by immunostaining of Cx43 and the gating function of GJs by dye spreading in neonatal rat cardiomyocytes (NRCMs) stimulated with these activators. We demonstrate that the Cx43 accumulation at cell–cell contacts depends on Epac and that dye spreading depends on PKA. Therefore, PKA and Epac downstream of cAMP cooperatively enhance functional GJ neoformation in cardiac myocytes.

Materials and Methods

Reagents and cAMP Analogs

Dibutyryl-cAMP (dbcAMP) was purchased from Sigma-Aldrich, Epac-specific activator 8-(4-chlorophenylthio)-2′-*O*-methyladenosine-3′,5′-cyclic monophosphate (8CPT) from Calbiochem; and PKA-specific activator N^6-benzoyladenosine-3′,5′-cyclic monophosphate (6Bnz) was from BIOLOG Life Science Institute. Other chemical compounds, antibodies, and adenoviruses are listed in the supplemental information (available online at http://circres.ahajournals.org).

Cell Culture

NRCMs were isolated from Wistar rats (1 to 2 days old; Kiwa Jikken Dobutsu, Japan) on a Percoll gradient as described previously.[20] The details of cardiac myocyte preparation are described in the supplemental information. The NRCMs spread onto the glass-base dishes for 24 hours after isolation were subjected to immunostaining or dye transfer assay after drug treatment for another 12 hours. We observed that the adherens junctions (AJs) were not maturated, although NRCMs contacted each other before the drug treatment, indicating that we used the reassembling NRCMs for the experiments. Experiments using animals were approved by our institutional animal use and care committee. All animal procedures were performed according to the *Guide for the Care and Use of Laboratory Animals* (NIH, revision 1996).

Immunocytochemistry

NRCMs stimulated with cAMP analogs were immunostained as described previously.[21] Briefly, cells cultured on glass-base dish were blocked with PBS containing 4% BSA for 1 hour at room temperature (RT), then stained with anti-Cx43, anti–sarcomeric α-actinin (S-αA), and anti–neural (N)-cadherin at RT. Protein reacting with primary antibodies was visualized with Alexa 488–labeled goat anti-rabbit IgG and Alexa 546–labeled goat anti-mouse IgG. Images were recorded with a confocal microscope (BX50WI; Olympus). For quantitative immunofluorescence analysis, images were also recorded using an epifluorescence microscope (IX-71; Olympus) controlled by MetaMorph version 6.2 software (Molecular Devices). The number of Cx43-positive dots at the cell–cell contacts on the fluorescence images were counted as Cx43 puncta.

Gating Function of GJs Analyzed by Microinjected Dye Transfer

Microinjected dye transfer was performed as described by Doble et al, with minor modifications.[22] The details of dye transfer method are described in the supplemental information.

RT-PCR Analysis

Total RNAs extracted from NRCMs and human cervical carcinoma cell line (HeLa) cells using Trizol (Invitrogen) were reverse-transcribed using SuperScript II and random primers (Invitrogen). The resultant DNAs were PCR-amplified using Epac-specific primers described in the supplemental information.

Western Blot Analysis and N-Cadherin Translocation Assay

NRCMs were lysed in buffer described in the supplemental information. Lysates precleared by centrifugation at 15 000*g* for 10 minutes were subjected to SDS-PAGE and immunoblotting with antibodies as indicated in Figures 3, 4, 5, and 6. Proteins reacting with primary antibodies were visualized by an enhanced chemiluminescence system (Amersham Biosciences) with peroxidase-conjugated and species-matched secondary antibodies and analyzed with an LAS-1000 system (Fuji Film). N-cadherin translocation assay was performed as described previously.[18]

Detection of GTP-Bound Form of Rap1

Rap1 activity was assessed by a modified Bos method as described previously.[23] Briefly, NRCMs starved in DMEM for 3 hours were treated with the stimulants as indicated in Figures 3 and 6 and lysed at 4°C in a pull-down lysis buffer described in the supplemental information. GTP-bound Rap1 was collected on glutathione *S*-transferase fused with Rap1 binding domain of Ral guanine nucleotide dissociation stimulator precoupled to glutathione-Sepharose beads and subjected to SDS-PAGE followed by immunoblotting using anti-Rap1.

Statistical Analysis

The results were expressed as the mean±SD. Student *t* test was used to analyze differences between two groups. Group differences were assessed with one-way ANOVA or two-way ANOVA, followed by post hoc comparisons tested with Scheffe's method. At least 3 fields randomly selected from each culture for analysis of Cx43 staining or at least 4 cells for dye transfer assay from each culture were used to yield a single value for each culture. The number of the cultures for analysis was indicated in the figure legends as n. Significant differences were indicated as P value <0.05 (*).

Results

cAMP Enhances Functional GJ Neoformation in Cultured NRCMs

Because cAMP has been reported previously to enhance GJ formation,[7] we confirmed the dbcAMP–regulated functional GJ neoformation by quantitatively analyzing Cx43 accumulation at the cell–cell contacts by immunostaining and gating function of GJs by microinjected dye transfer assay. dbcAMP enhanced the Cx43 accumulation at the cell–cell contacts (Figure 1A and 1B). To neglect the possibility of cardiac fibroblast contamination in the NRCMs in the following

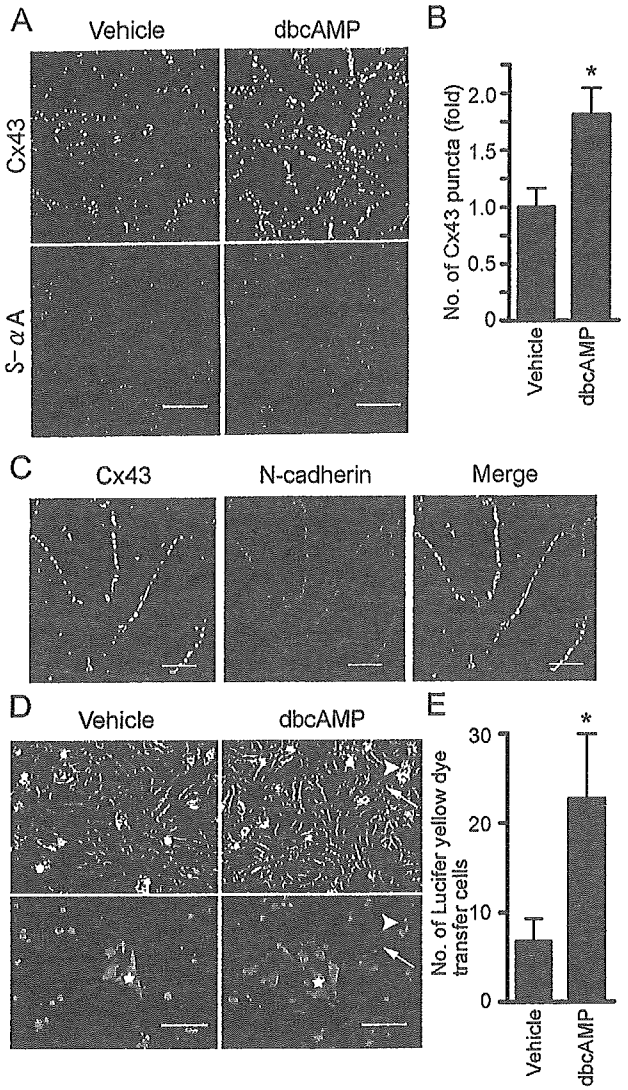

Figure 1. cAMP induces Cx43 accumulation at cell–cell contacts and enhances gap junctional intercellular communication. A, NRCMs cultured 24 hours after cell preparation were stimulated with vehicle or 1 mmol/L dbcAMP for 12 hours. Cells were stained with anti-Cx43 (green) and anti-S-αA (red). Images were obtained through a confocal microscope (BX50WI). Bar=20 μm. B, NRCMs stimulated by dbcAMP were analyzed for Cx43 accumulation by counting the number of puncta at cell–cell contacts. Mean number±SD is expressed as fold increase relative to that observed in the cell treated with vehicle. *P<0.05 vs vehicle as analyzed by Student's t test (n=4). Three fields randomly selected from each culture were used for measuring the fold activation between vehicle- and dbcAMP-treated culture by counting Cx43-positive puncta. C, Cells treated with dbcAMP were immunostained with anti-Cx43 (green) and anti–N-cadherin (red). A merged image is shown on the right. Note that puncta for Cx43 are localized to cell–cell contacts as indicated by the N-cadherin immunostaining. Bar=5 μm. D, Microinjected dye transfer assay shows the extent of dye transferring between neighboring cells through GJs. NRCMs stimulated with 1 mmol/L dbcAMP for 12 hours were microinjected with 10% Lucifer yellow. Cells 3 minutes after dye injection were phase contrast imaged (top panels) and fluorescence imaged (bottom panels). Asterisks indicate dye-injected cells. Arrows and arrowheads denote typical dye-transferred cell and cell debris emitting nonspecific fluorescence, respectively. Bar=50 μm. E, Quantitative analysis of D is shown as mean number of dye-positive cells in either vehicle or dbcAMP-treated NRCMs. *P<0.05 as analyzed by Student's t test (n=6).

experiments, and to show the confluence of the NRCMs, cells were immunostained for sarcomeric α-actinin (Figure 1A, bottom). The Cx43 puncta in the cells treated with dbcAMP for 12 hours were clearly observed at the cell–cell contacts, where N-cadherin localized (Figure 1C), indicating that dbcAMP induces the accumulation of Cx43 at the cell–cell contacts. We investigated the effect of dbcAMP on gating function of GJs by microinjected dye transfer assays (Figure 1D and 1E). Microinjected dye was more widely transferred to the neighboring cells in dbcAMP-treated NRCMs than vehicle-treated cells (Figure 1D). The quantitative data are shown in Figure 1E. These results are in agreement with previous reports[7,8] and validated the assays we used in this study.

PKA Is Required But Not Sufficient Alone for cAMP-Enhanced GJ Neoformation

Because PKA is involved in the enhancement of GJ formation,[15] we first tested the effect of H89, a specific PKA inhibitor, on cAMP-enhanced accumulation of Cx43. Unexpectedly, H89 did not block the dbcAMP-induced accumulation of Cx43 (Figure 2A and 2B), although H89 did block cAMP-enhanced intercellular communication assessed by microinjected dye transfer assays (Figure 2C).

We next examined the effect of 6Bnz, a specific activator for PKA,[24] on intercellular communication and Cx43 accumulation at cell–cell contacts to directly assess the involvement of PKA in cAMP-enhanced GJ formation. 6Bnz induced Cx43 accumulation slightly but to a much lesser extent than dbcAMP (Figure 2D and 2E). Notably, 6Bnz enhanced dye transfer to a greater extent than vehicle but to a lesser extent than dbcAMP (Figure 2F). These results indicate that PKA signaling is required but not sufficient alone for cAMP-enhanced GJ neoformation and suggest that there is a novel signaling downstream of cAMP in addition to PKA involved in Cx43 accumulation at cell–cell contacts for functional GJ neoformation.

cAMP Activates PKA and Epac-Rap1 Signaling in NRCMs

Epac has been identified as a novel cAMP target and a Rap1-specific GEF. We therefore hypothesized that Epac-Rap1 signaling may be involved in cAMP-enhanced GJ neoformation. RT-PCR analysis revealed the expression of Epac in NRCM but not in HeLa cells used as a negative control (Figure 3A). To test the hypothesis, we first examined whether dbcAMP induces the activation of Rap1 and the phosphorylation of cAMP response element binding protein (CREB) in NRCMs. As shown in Figure 3B, dbcAMP induced Rap1 and CREB activation in NRCMs. Rap1 activation by dbcAMP is dependent on time and concentration (supplemental Figure IA and IB, available online at http://circres.ahajournals.org). H89 inhibited dbcAMP-induced CREB phosphorylation but not dbcAMP-induced Rap1 activation (Figure 3B and 3C), indicating that Rap1 activation does not depend on PKA, whereas CREB phosphorylation depends exclusively on PKA. We next tested whether Rap1 activation and CREB phosphorylation are induced by 8CPT, which has been developed recently as a specific activator for Epac.[25] 8CPT only activated Rap1, not CREB. In striking contrast, 6Bnz induced CREB activation but did not affect

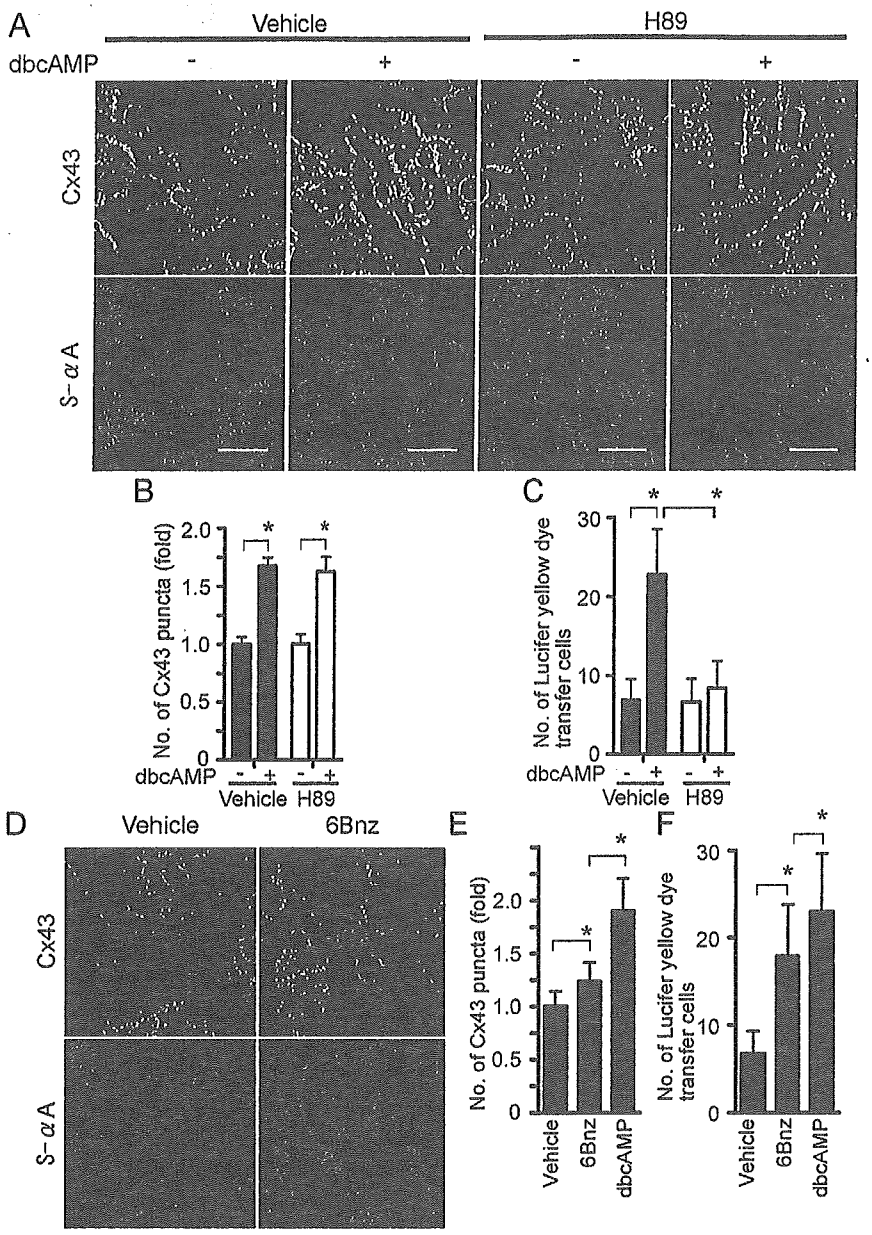

Figure 2. PKA signaling mainly contributes to gating function of GJs. A, NRCMs pretreated with or without 5 μmol/L H89 for 30 minutes were stimulated with or without 1 mmol/L dbcAMP in the presence or absence of 5 μmol/L H89 for 12 hours. After the stimulation, cells were immunostained with anti-Cx43 and anti-S-αA as described in Figure 1A legend. Bar=20 μm. B, Cx43 accumulation in cells treated as in A was quantitatively analyzed. Statistical significance between groups was analyzed by two-way ANOVA with Scheffe's method, indicating that the factor of with/without dbcAMP is significant but not that of vehicle/H89 (*P<0.05; n=6) C, Effect of H89 on dbcAMP-enhanced gap junctional intercellular communication was evaluated by microinjected dye transfer assay as described in Figure 1E legend. Statistical significance between groups was analyzed by two-way ANOVA with Scheffe's method, indicating that both factors, with/without dbcAMP and vehicle/H89, are significant (*P<0.05; n=6). D, NRCMs were stimulated with either vehicle or 1 mmol/L 6Bnz for 12 hours and immunostained with anti-Cx43 and anti-S-αA. Bar=20 μm. E, The effect of 1 mmol/L 6Bnz on Cx43 accumulation at the cell–cell contacts was evaluated similarly to Figure 1B. Statistical significance between groups was analyzed by one-way ANOVA with Scheffe's method (*P<0.05; n=4). F, The effect of 6Bnz on junctional intercellular communication between NRCMs was similarly evaluated by microinjected dye transfer assay to the Figure 1D. Statistical significance was evaluated by one-way ANOVA with Scheffe's method (*P<0.05; n=4).

Rap1 activity (Figure 3D and 3E). Together, these findings demonstrate that cAMP activates Epac-Rap1 and PKA signaling pathways in NRCMs.

Activation of Epac Signaling Leads to Cx43 Accumulation at Cell–Cell Contacts

Because we observed Rap1 activation in response to dbcAMP, we proceeded to investigate the involvement of Epac-Rap1 signaling in cAMP-induced Cx43 accumulation at cell–cell contacts. Like dbcAMP, 8CPT significantly enhanced the accumulation of Cx43 at the cell–cell contacts (Figure 4A and 4B). 8CPT induced Cx43 accumulation at the cell–cell contacts to a similar extent to dbcAMP and to a greater extent than 6Bnz. 6Bnz only slightly increased the number of Cx43 puncta (Figure 4B) compared with vehicle and did not further increase the accumulation of Cx43 at cell–cell contacts caused by 8CPT alone. These results indicate that Epac-mediated signaling is mainly responsible for cAMP-induced Cx43 accumulation at the cell–cell contacts.

We excluded the possibility that increased synthesis of Cx43 on cAMP stimulation resulted in the accumulation of Cx43 at the cell–cell contacts. No discernible increase was observed in the cells stimulated with vehicle, dbcAMP, 8CPT, 6Bnz, and a combination of 8CPT and 6Bnz for 12 hours (Figure 4C and 4D), suggesting that distribution or functional augmentation of GJs is essential for cAMP-induced functional GJ neoformation. In addition, phosphorylation of Cx43 was not affected by dbcAMP, 8CPT, or 6Bnz, nor a combination of 8CPT and 6Bnz (Figure 4C and 4E).

Epac Enhances AJ Formation

Several lines of evidence suggest that AJ formation organized by N-cadherin is a prerequisite for GJ assembly in cardiomyocytes when reassembling and recoupling.[26–28] We used reassembling NRCMs before drug treatment. Recently, we and others revealed that Rap1 is involved in the cell–cell contacts mediated by epithelial (E)-cadherins and vascular

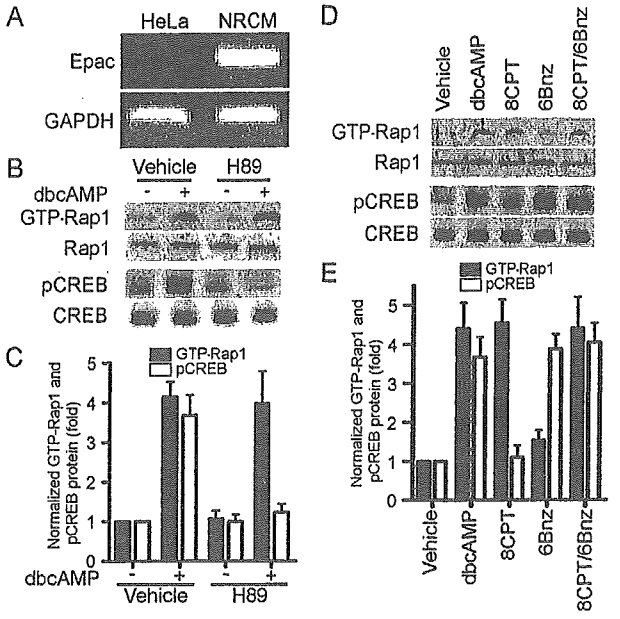

Figure 3. cAMP induces Epac-Rap1 signal as well as PKA signal in NRCMs. A, RT-PCR analysis shows the expression of Epac in NRCMs but not in HeLa cells (used as a negative control). GAPDH was shown as a positive control for RT-PCR. B, Serum-starved NRCMs were stimulated with 1 mmol/L dbcAMP in the absence or presence of H89 for 15 minutes. GTP-bound Rap1 were assessed by pull-down assay. Phosphorylation of CREB was analyzed by Western blot analysis using anti-CREB and anti-phospho-CREB (pCREB). A representative result of 3 independent experiments is shown. C, Data obtained from 4 independent experiments were analyzed quantitatively. Fold activation indicates the ratio of the poststimulation GTP-Rap1 and pCREB intensity of total Rap1 and CREB intensity to the prestimulation GTP-Rap1 and pCREB intensity of total Rap1 and CREB intensity. D, Serum-starved NRCMs were stimulated with either vehicle, 1 mmol/L dbcAMP, 1 mmol/L 8CPT, 1 mmol/L 6Bnz, or 1 mmol/L 8CPT and 1 mmol/L 6Bnz for 15 minutes. GTP-bound Rap1 and phosphorylation of CREB were assessed as described in B. E, Data obtained from 4 independent experiments were analyzed similarly to C.

endothelial–cadherins (VE-cadherins).[18,29] Thus, it is possible that cAMP enhances GJ neoformation by enhancing N-cadherin–mediated AJ formation preceding the GJ formation in NRCMs. To address this possibility, we investigated whether cAMP induces N-cadherin–mediated AJ formation in NRCMs. N-cadherin distribution at cell–cell contacts was enhanced by dbcAMP and 8CPT, whereas 6Bnz neither affected the distribution of N-cadherin nor enhanced the effect of 8CPT (Figure 5A).

To quantitatively analyze the localization of N-cadherin after drug treatment, we performed a biochemical N-cadherin translocation assay. Because N-cadherin is connected to actin cytoskeleton in maturated AJs, cadherin anchored to actin cytoskeleton can be detected in detergent-insoluble fractions of cell lysates. We found an increase in N-cadherin in Triton X-100–insoluble fraction when stimulated by dbcAMP and 8CPT (Figure 5B). However, 6Bnz did not change either basal- or 8CPT-increased levels of N-cadherin in the Triton X-100–insoluble fraction (Figure 5B and 5C). Collectively, these findings indicate that cAMP enhances AJ formation through Epac in NRCMs. We found no difference in N-cadherin expression in NRCMs stimulated with dbcAMP, 8CPT, or 6Bnz, or a combination of 8CPT and 6Bnz by immunoblotting (data not shown).

Rap1 Activation Is Essential for cAMP-Mediated Cx43 Redistribution and AJ Formation

We investigated the role of Rap1 in cAMP-induced Cx43 accumulation and AJ formation in NRCMs. To examine the effect of Rap1 on AJ and GJ formation, we inactivated Rap1 by adenovirus-expressing Rap1GAP1b, which specifically catalyzes the hydrolysis of GTP to GDP on Rap1.[30] Endogenous Rap1 activity was almost completely suppressed by the expression of increasing amount of Rap1GAP1b in NRCMs (Figure 6A). Moreover, overexpression of Rap1GAP1b inhibited cAMP-induced Rap1 activity without affecting cAMP-stimulated CREB phosphorylation (Figure 6B), confirming that Rap1GAP1b specifically blocks Epac-Rap1 pathway but not PKA-mediated signaling.

Inactivation of Rap1 blocked the cAMP-induced accumulation of Cx43 and N-cadherin at the cell–cell contacts (Figure 6C and 6D). dbcAMP-induced translocation of N-cadherin to cytoskeleton-anchored fraction was inhibited by inactivation of Rap1 but not by LacZ overexpression (Figure 6E and 6F). These results suggest that cAMP induces N-cadherin–based AJ assembly through an Epac-Rap1 signaling pathway, which may precede the accumulation of Cx43-based GJs.

PKA and Epac-Rap1 Signaling Cooperatively Enhances GJ Neoformation in NRCMs

Because we found that PKA alone is not sufficient for cAMP-enhanced GJ neoformation and that Epac-Rap1 signaling is involved in cAMP-induced accumulation of Cx43, we assessed the effect of PKA activation and Epac-Rap1 activation on gating function of GJs. 8CPT merely showed the weak enhancement of the intercellular connection, as revealed by microinjected dye transfer assay (Figure 7A). However, 8CPT significantly enhanced 6Bnz-mediated intercellular communication (Figure 7B). The effect of the combination of 8CPT and 6Bnz was comparable to that of dbcAMP. Given that 8CPT induces the Cx43 accumulation at the cell–cell contacts, cAMP potentiates functional GJ neoformation via a PKA-mediated enhanced gating function and Epac-Rap1 signal-mediated accumulation of Cx43 to cell–cell contacts.

Discussion

The function of GJs in the heart depends on the number of GJs between neighboring cells and the gating function of individual GJ at the cell–cell contacts. We investigated how cAMP induces Cx43 accumulation at cell–cell contacts and enhances gating function in NRCMs that were about to develop the mature cell–cell contacts. For the first time, we demonstrated the involvement of Epac-Rap1 signaling downstream of cAMP in GJ neoformation of cardiomyocytes. Although Cx43 accumulated at the cell–cell contacts on cAMP stimulation has been ascribed to PKA,[7] this study demonstrated that Epac-Rap1 signaling activated by cAMP is mainly responsible for the redistribution of Cx43 to cell–cell contacts.

The number of GJs was increased by Epac-Rap1 downstream of cAMP as indicated by the increase in Cx43-positive puncta at cell–cell contacts. However, there was no increase in the amount of Cx43 after cAMP treatment, indicating the importance of the redistribution of Cx43 rather than increase of Cx43 transcription on cAMP. How does Epac signaling induce the accumulation of Cx43 at cell–cell contacts?

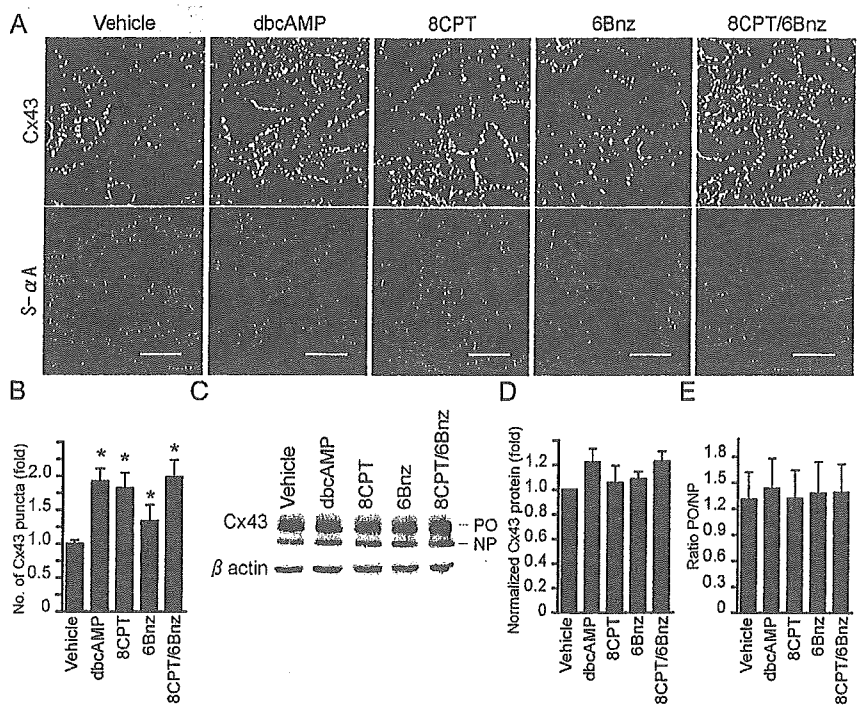

Figure 4. Activation of Epac signaling induces Cx43 accumulation at cell–cell contacts. A, NRCMs stimulated for 12 hours with drugs as indicated at the top were stained with anti-Cx43 and anti-S-αA as described in Figure 1A legend. Bar=20 μm. B, Cx43 accumulation was quantitatively analyzed in Figure 1B. Significant differences between vehicle-treated cells and all drug-treated cells was analyzed by one-way ANOVA with Scheffe's method (*$P<0.05$; n=6). C, NRCMs stimulated as indicated at the top were examined for Cx43 by Western blot analysis. Upper and lower bands correspond to phosphorylated (PO) and nonphosphorylated (NP) Cx43, respectively. D, Total Cx43 (phosphorylated and nonphosphorylated) expression of NRCMs treated for 12 hours with drugs as indicated at the bottom was quantitatively analyzed by three independent Western blot analyses for Cx43. The intensity of the drug-stimulated Cx43 normalized by β-catenin divided by that of vehicle-stimulated Cx43 was expressed as fold activation. E, The ratio is expressed by the intensity of phosphorylated Cx43 (PO) divided by that of nonphosphorylated Cx43 (NP).

Epac-Rap1 activation resulted in enhancement of AJ formation accompanied by GJ formation, as evidenced by increases in N-cadherin and Cx43 at the cell–cell contacts after dbcAMP stimulation (Figure 5). AJ formation constituted by N-cadherin is a prerequisite for GJ neoformation.[28,31] When adult myocytes are cultured, Cx43 is transported and accumulated at the plasma membrane, where N-cadherin accumulates on cell–cell contact.[26] Therefore, GJ formation depends on N-cadherin–based AJ maturation. We have shown previously that the Epac-Rap1 signal enhances the VE-cadherin–based cell–cell contacts in vascular endothelial cells.[18] In this study, we found that Epac activation resulted in the increased accumulation of N-cadherin at the intercellular junction of NRCMs. Thus, N-cadherin accumulation at the cell–cell contacts induced by the Epac-Rap1 signal may account for Cx43 accumulation in NRCMs by analogy to Epac-Rap1–triggered VE-cadherin accumulation in vascular endothelial cells.

The target of activated Rap1 for enhancement of cadherin-based AJ is still unclear. Rac belonging to Rho family GTPase and regulating actin cytoskeleton is suggested to function downstream of Rap1.[32] Therefore, Rac may increase the chances of cell contacts and induce cadherin engagement by extending membrane downstream of Rap1. Maturated N-cadherin on Epac activation, which is detected in the cytoskeleton-anchored fraction, may be accompanied by translocation of Cx43 through cadherin-associating β-catenin

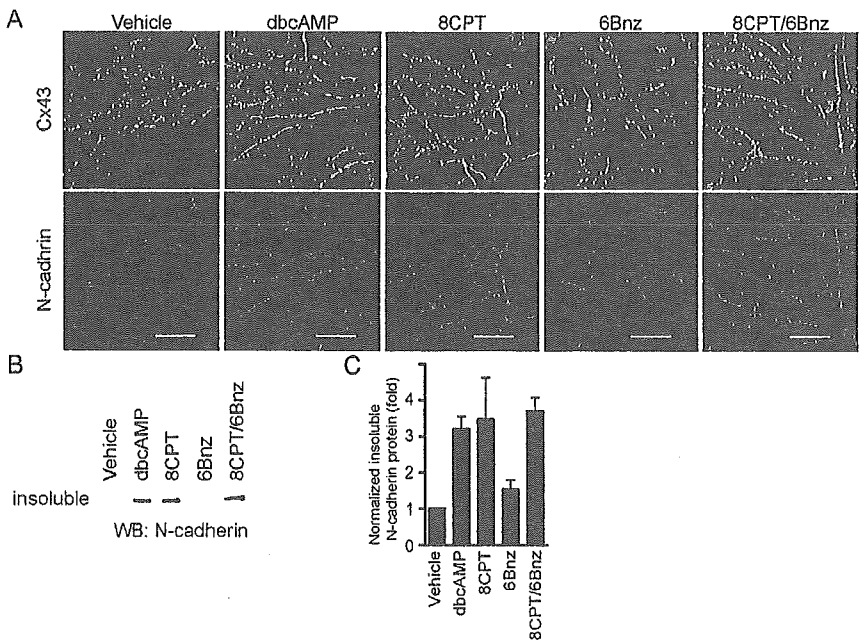

Figure 5. Activation of Epac induces AJ formation. A, NRCMs stimulated for 12 hours with drugs as indicated at the top were immunostained with anti-Cx43 (green) and anti-N-cadherin (red). Bar=20 μm. B, NRCMs stimulated as in A were fractionated with cytoskeleton stabilizing buffer. Triton X-100–insoluble fraction was subjected to SDS-PAGE followed by Western blot analysis (WB) with anti-N-cadherin. A representative result of three independent experiments is shown. C, The data obtained from three independent experiments of B was quantitatively analyzed. The result is indicated as fold increase calculated by dividing the amount of insoluble N-cadherin from the cells treated with the drug by that from the cells treated with vehicle.

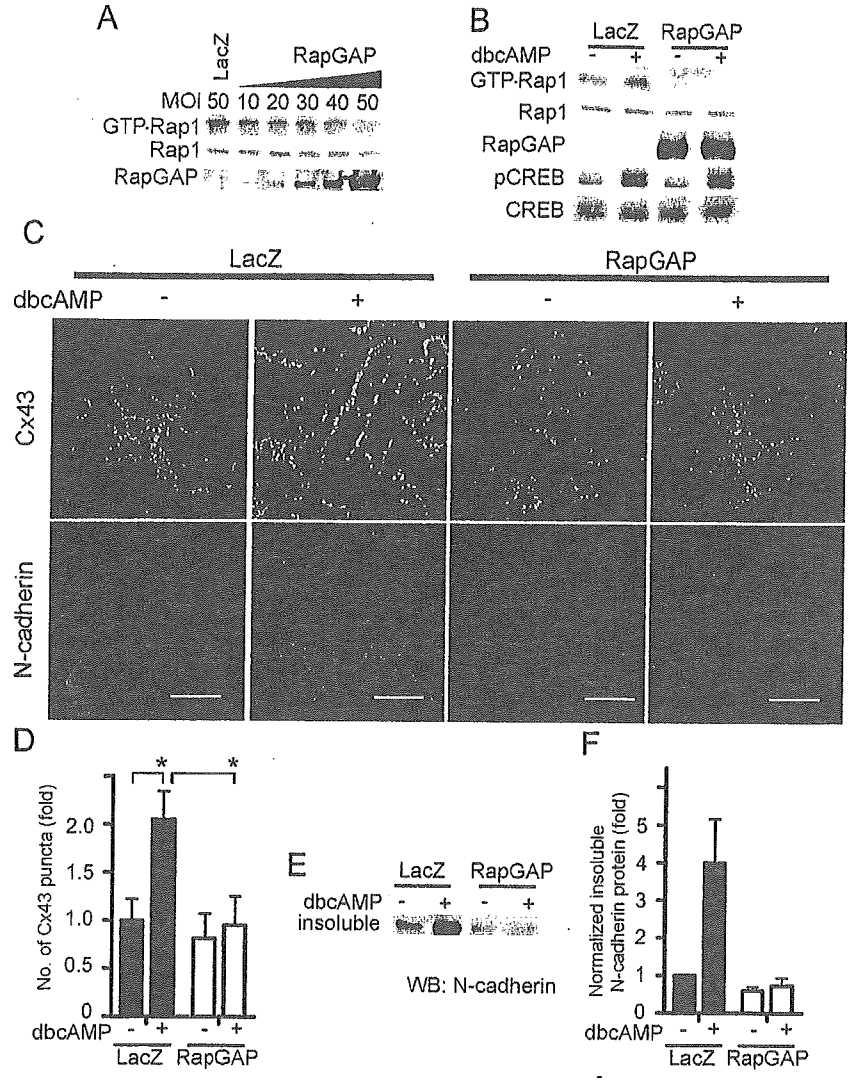

Figure 6. Rap1 activation is required for cAMP-induced Cx43 accumulation at the cell–cell contacts and AJ formation. A, Rap1 inactivation by Rap1GAP1b was verified by detecting GTP-Rap1 in NRCMs infected with different multiplicity of infection (MOI) of adenovirus-expressing Rap1GAP1b (Ad-RapGAP). An adenovirus-expressing LacZ (Ad-LacZ) at 50 MOI was used as a control. GTP-Rap1 was detected by pull-down assay. Rap1 and Rap1GAP1b (RapGAP) expression was examined by Western blot analysis using antibodies as indicated at the left. B, NRCMs infected with either Ad-LacZ or Ad-RapGAP at an MOI of 50 for 24 hours were stimulated with vehicle (−) or 1 mmol/L dbcAMP (+) for 15 minutes and analyzed for Rap1 and CREB activation. C, Localization of N-cadherin and Cx43 was examined similarly to Figure 5A in NRCMs infected with Ad-LacZ or Ad-RapGAP after stimulated with vehicle or 1 mmol/L dbcAMP for 12 hours. Bar=20 μm. D, The effect of inactivation of Rap1 on dbcAMP-induced accumulation of Cx43 was analyzed by two-way ANOVA with Scheffe's method, indicating that both factors, with/without dbcAMP and LacZ/RapGAP, are significant (*P<0.05; n=6). E, Translocation of N-cadherin was examined in NRCMs infected with Ad-LacZ or Ad-RapGAP after stimulation of dbcAMP. A representative of three independent results is shown. F, The three independent results from D were analyzed similarly to Figure 5C.

because Cx43 is capable of binding to β-catenin.[14] Because ZO-1 is recruited to AJs by binding to α-catenin and is also capable of binding to Cx43,[33] ZO-1 may participate in the accumulation of Cx43 during maturation of AJs.

Another factor affecting functional GJ neoformation in addition to the number of GJs is the gating function of individual GJs. PKA activation facilitates intercellular communication without accumulation of Cx43 at cell–cell contacts, concurring with previous reports underpinning that PKA and cAMP increases single channel conductance of the GJ,[34] although the characteristics of single GJ channel conductance evoked by PKA activation still remains elusive.[15] We found a marked increase in dye transfer on PKA activation with a slightly increased accumulation of Cx43 at the cell–cell contacts (Figures 4 and 7). These results indicate that PKA mainly contributes to the functional neoformation of GJs by enhancing gating function of GJs. Phosphorylation of Cx43 on Ser residues is required for intercellular communication of GJs.[35] Because we found no significant increase in either total Cx43 or phosphorylated Cx43, PKA may indirectly modulate GJ conductance in addition to direct phosphorylation of Cx43 or may phosphorylate a critical Ser/Thr that was indistinguishable in the phosphorylated Cx43 band in our immunoblot for Cx43 (Figure 4C).

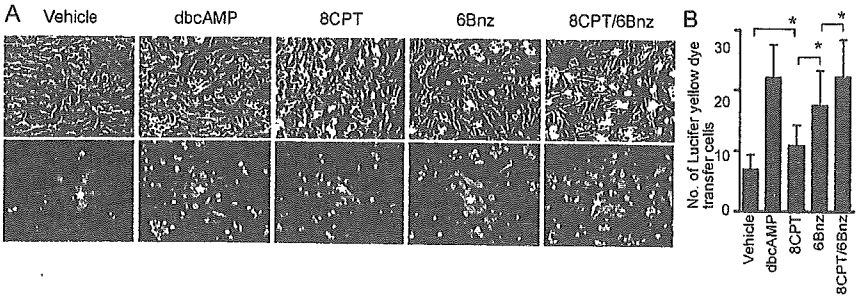

Figure 7. PKA signal and Epac-Rap1 signal cooperatively enhance intercellular communication through GJs. A, Intercellular communication was assessed by microinjected dye transfer assay using NRCMs stimulated with drugs as indicated at the top. B, Dye spread was quantitatively analyzed similarly to Figure 2F. Statistical significance between groups was evaluated by one-way ANOVA with Scheffe's method (*P<0.05; n=6).

The enhanced gating function of GJs is mainly ascribed to PKA, whereas the accumulation of Cx43 to cell–cell contacts is mainly attributable to Epac-Rap1 signal. Hence, Epac-Rap1 signal may accelerate the trafficking of Cx43 to the plasma membrane or inhibit the endocytosis of Cx43 from the plasma membrane. We did not quantify the translocation of Golgi fraction to cell–cell contacts on cAMP stimulation. Previously, GJ trafficking was dynamically monitored by green fluorescence protein–tagged Cx43.[36] Therefore, it will be of great interest to observe the Cx43 dynamics on 8CPT stimulation to directly elucidate Epac-Rap1 signaling.

In conclusion, we demonstrated that cAMP potentiates functional GJ neoformation by a PKA-dependent increase in intercellular communication and by an Epac-Rap1–dependent accumulation of Cx43 in NRCMs.

Acknowledgments

This work was supported in part by grants from the Ministry of Health, Labor, and Welfare Foundation of Japan; the Ministry of Education, Science, Sports, and Culture of Japan; the Promotion of Fundamental Studies in Health Science of the Organization for Pharmaceutical Safety and Research of Japan; the Japan Health Science Foundation; and Astellas Foundation for Research on Metabolic Disorders. We thank Michiyuki Matsuda and Akihiro Umezawa for their helpful input; Nobuo Shirahashi for statistical analysis; James T. Pearson and Michael E. Mendelsohn for critical reading; and Yuko Matsuura and Manami Sone for their technical assistance.

References

1. Yeager M. Structure of cardiac gap junction intercellular channels. *J Struct Biol.* 1998;121:231–245.
2. Sohl G, Willecke K. Gap junctions and the connexin protein family. *Cardiovasc Res.* 2004;62:228–232.
3. Vozzi C, Dupont E, Coppen SR, Yeh HI, Severs NJ. Chamber-related differences in connexin expression in the human heart. *J Mol Cell Cardiol.* 1999;31:991–1003.
4. Davis LM, Rodefeld ME, Green K, Beyer EC, Saffitz JE. Gap junction protein phenotypes of the human heart and conduction system. *J Cardiovasc Electrophysiol.* 1995;6:813–822.
5. Saffitz JE, Kleber AG. Effects of mechanical forces and mediators of hypertrophy on remodeling of gap junctions in the heart. *Circ Res.* 2004;94:585–591.
6. Gutstein DE, Morley GE, Fishman GI. Conditional gene targeting of connexin43: exploring the consequences of gap junction remodeling in the heart. *Cell Commun Adhes.* 2001;8:345–348.
7. Darrow BJ, Fast VG, Kleber AG, Beyer EC, Saffitz JE. Functional and structural assessment of intercellular communication. Increased conduction velocity and enhanced connexin expression in dibutyryl cAMP-treated cultured cardiac myocytes. *Circ Res.* 1996;79:174–183.
8. Paulson AF, Lampe PD, Meyer RA, TenBroek E, Atkinson MM, Walseth TF, Johnson RG. Cyclic AMP and LDL trigger a rapid enhancement in gap junction assembly through a stimulation of connexin trafficking. *J Cell Sci.* 2000;113:3037–3049.
9. Saffitz JE, Laing JG, Yamada KA. Connexin expression and turnover: implications for cardiac excitability. *Circ Res.* 2000;86:723–728.
10. Lampe PD, TenBroek EM, Burt JM, Kurata WE, Johnson RG, Lau AF. Phosphorylation of connexin43 on serine368 by protein kinase C regulates gap junctional communication. *J Cell Biol.* 2000;149:1503–1512.
11. TenBroek EM, Lampe PD, Solan JL, Reynhout JK, Johnson RG. Ser364 of connexin43 and the upregulation of gap junction assembly by cAMP. *J Cell Biol.* 2001;155:1307–1318.
12. Lin R, Warn-Cramer BJ, Kurata WE, Lau AF. v-Src phosphorylation of connexin 43 on Tyr247 and Tyr265 disrupts gap junctional communication. *J Cell Biol.* 2001;154:815–827.
13. Toyofuku T, Yabuki M, Otsu K, Kuzuya T, Hori M, Tada M. Direct association of the gap junction protein connexin-43 with ZO-1 in cardiac myocytes. *J Biol Chem.* 1998;273:12725–12731.
14. Ai Z, Fischer A, Spray DC, Brown AM, Fishman GI. Wnt-1 regulation of connexin43 in cardiac myocytes. *J Clin Invest.* 2000;105:161–171.
15. Schulz R, Heusch G. Connexin 43 and ischemic preconditioning. *Cardiovasc Res.* 2004;62:335–344.
16. Kawasaki H, Springett GM, Mochizuki N, Toki S, Nakaya M, Matsuda M, Housman DE, Graybiel AM. A family of cAMP-binding proteins that directly activate Rap1. *Science.* 1998;282:2275–2279.
17. de Rooij J, Zwartkruis FJ, Verheijen MH, Cool RH, Nijman SM, Wittinghofer A, Bos JL. Epac is a Rap1 guanine-nucleotide-exchange factor directly activated by cyclic AMP. *Nature.* 1998;396:474–477.
18. Fukuhara S, Sakurai A, Sano H, Yamagishi A, Somekawa S, Takakura N, Saito Y, Kangawa K, Mochizuki N. Cyclic AMP potentiates vascular endothelial cadherin-mediated cell-cell contact to enhance endothelial barrier function through an Epac-Rap1 signaling pathway. *Mol Cell Biol.* 2005;25:136–146.
19. Cullere X, Shaw SK, Andersson L, Hirahashi J, Luscinskas FW, Mayadas TN. Regulation of vascular endothelial barrier function by Epac, a cAMP-activated exchange factor for Rap GTPase. *Blood.* 2005;105:1950–1955.
20. Oyamada Y, Zhou W, Oyamada H, Takamatsu T, Oyamada M. Dominant-negative connexin43-EGFP inhibits calcium-transient synchronization of primary neonatal rat cardiomyocytes. *Exp Cell Res.* 2002;273:85–94.
21. Ogita H, Kunimoto S, Kamioka Y, Sawa H, Masuda M, Mochizuki N. EphA4-mediated Rho activation via Vsm-RhoGEF expressed specifically in vascular smooth muscle cells. *Circ Res.* 2003;93:23–31.
22. Doble BW, Chen Y, Bosc DG, Litchfield DW, Kardami E. Fibroblast growth factor-2 decreases metabolic coupling and stimulates phosphorylation as well as masking of connexin43 epitopes in cardiac myocytes. *Circ Res.* 1996;79:647–658.
23. Ohba Y, Ikuta K, Ogura A, Matsuda J, Mochizuki N, Nagashima K, Kurokawa K, Mayer BJ, Maki K, Miyazaki J, Matsuda M. Requirement for C3G-dependent Rap1 activation for cell adhesion and embryogenesis. *EMBO J.* 2001;20:3333–3341.
24. Christensen AE, Selheim F, de Rooij J, Dremier S, Schwede F, Dao KK, Martinez A, Maenhaut C, Bos JL, Genieser HG, Doskeland SO. cAMP analog mapping of Epac1 and cAMP kinase. Discriminating analogs demonstrate that Epac and cAMP kinase act synergistically to promote PC-12 cell neurite extension. *J Biol Chem.* 2003;278:35394–35402.
25. Enserink JM, Christensen AE, de Rooij J, van Triest M, Schwede F, Genieser HG, Doskeland SO, Blank JL, Bos JL. A novel Epac-specific cAMP analogue demonstrates independent regulation of Rap1 and ERK. *Nat Cell Biol.* 2002;4:901–906.
26. Hertig CM, Butz S, Koch S, Eppenberger-Eberhardt M, Kemler R, Eppenberger HM. N-cadherin in adult rat cardiomyocytes in culture. II. Spatio-temporal appearance of proteins involved in cell-cell contact and communication. Formation of two distinct N-cadherin/catenin complexes. *J Cell Sci.* 1996;109:11–20.
27. Kostetskii I, Li J, Xiong Y, Zhou R, Ferrari VA, Patel VV, Molkentin JD, Radice GL. Induced deletion of the N-cadherin gene in the heart leads to dissolution of the intercalated disc structure. *Circ Res.* 2005;96:346–354.
28. Kostin S, Hein S, Bauer EP, Schaper J. Spatiotemporal development and distribution of intercellular junctions in adult rat cardiomyocytes in culture. *Circ Res.* 1999;85:154–167.
29. Hogan C, Serpente N, Cogram P, Hosking CR, Bialucha CU, Feller SM, Braga VM, Birchmeier W, Fujita Y. Rap1 regulates the formation of E-cadherin-based cell-cell contacts. *Mol Cell Biol.* 2004;24:6690–6700.
30. Mochizuki N, Ohba Y, Kiyokawa E, Kurata T, Murakami T, Ozaki T, Kitabatake A, Nagashima K, Matsuda M. Activation of the ERK/MAPK pathway by an isoform of rap1GAP associated with G alpha(i). *Nature.* 1999;400:891–894.
31. Volk T, Geiger B. A 135-kDa membrane protein of intercellular adherens junctions. *EMBO J.* 1984;3:2249–2260.
32. Maillet M, Robert SJ, Cacquevel M, Gastineau M, Vivien D, Bertoglio J, Zugaza JL, Fischmeister R, Lezoualc'h F. Crosstalk between Rap1 and Rac regulates secretion of sAPPalpha. *Nat Cell Biol.* 2003;5:633–639.
33. Itoh M, Nagafuchi A, Moroi S, Tsukita S. Involvement of ZO-1 in cadherin-based cell adhesion through its direct binding to alpha catenin and actin filaments. *J Cell Biol.* 1997;138:181–192.
34. De Mello WC. Impaired regulation of cell communication by beta-adrenergic receptor activation in the failing heart. *Hypertension.* 1996;27:265–268.
35. Duncan JC, Fletcher WH. Alpha-1 connexin (connexin43) gap junctions and activities of cAMP-dependent protein kinase and protein kinase C in developing mouse heart. *Dev Dyn.* 2002;223:96–107.
36. Lauf U, Giepmans BN, Lopez P, Braconnot S, Chen SC, Falk MM. Dynamic trafficking and delivery of connexons to the plasma membrane and accretion to gap junctions in living cells. *Proc Natl Acad Sci U S A.* 2002;99:10446–10451.

Long-Term and Sustained COMP-Angl Induces Long-Lasting Vascular Enlargement and Enhanced Blood Flow

Chung-Hyun Cho, Kyung Eun Kim, Jonghoe Byun, Hyung-Suk Jang, Duk-Kyung Kim, Peter Baluk, Fabienne Baffert, Gyun Min Lee, Naoki Mochizuki, Jin Kim, Byeong Hwa Jeon, Donald M. McDonald, Gou Young Koh

Abstract—Vascular enlargement is a characteristic feature of angiopoietin-1 (Ang1)-induced changes in adult blood vessels. However, it is unknown whether tissues having Ang1-mediated vascular enlargement have more blood flow or whether the enlargement is reversible. We have recently created a soluble, stable and potent Ang1 variant, COMP-Ang1. In the present study, we investigated the effects of varied dose and duration of COMP-Ang1 on vascular enlargement and blood flow in the tracheal microvasculature of adult mice and explored a possible mechanism of long-lasting vascular enlargement. We found that COMP-Ang1 administered by adenoviral vector induced long-lasting vascular enlargement and increased tracheal blood flow. In contrast, short-term administration of COMP-Ang1 recombinant protein induced transient vascular enlargement that spontaneously reversed within a month. In both cases, the vascular enlargement resulted from endothelial proliferation. The COMP-Ang1–induced vascular remodeling is mediated mainly through Tie2 activation. Sustained overexpression of Tie2 could participate in the maintenance of vascular changes. Together, our findings indicate that sustained treatment with COMP-Ang1 can produce long-lasting vascular enlargement and increased blood flow. (***Circ Res.* 2005;97:86-94.**)

Key Words: angiopoietin-1 ■ COMP-Ang1 ■ vascular enlargement ■ blood flow

Angiopoietin-1 (Ang1) is known to be a ligand to Tie2 tyrosine kinase receptor expressed on endothelial cells.[1] Ang1/Tie2 signaling is thought be involved in branching and remodeling of the primitive vascular network and in the recruitment of mural cells during development.[2,3] Transgenic overexpression of Ang1 using the skin-specific keratin-14 promoter produces leakage-resistant and enlarged vessels with an increased number of endothelial cells in skin.[4,5] Gene transfer of Ang1 into ischemic tissues produces notably enlarged blood vessels.[6,7] Baffert et al recently identified that Ang1-induced vascular enlargement could be the result of endothelial proliferation in trachea mucosa.[8] Thus, a cardinal feature of Ang1-induced vascular remodeling is vascular enlargement resulting from endothelial cell proliferation in adult animals.[4–8]

Given that Ang1-induced therapeutic benefits correlated with vascular enlargement in the ischemic tissues,[6,7,9] enhanced blood flow through blood vessels enlarged by Ang1 treatment could provide a great therapeutic benefit to ischemic peripheral tissues. However, it is not known whether the tissues having Ang1-mediated enlarged vessels have more blood flow. In addition, the effective dose and treatment period of Ang1 for inducing effective vascular enlargement is not known. Moreover, it is not known whether Ang1-mediated vascular enlargement regresses when Ang1 stimulation is withdrawn.

We have recently developed a soluble, stable, and potent Ang1 variant, COMP-Ang1.[10] To create this protein, we replaced the amino-terminal portion of Ang1 with the short coiled-coil domain of cartilage oligomeric matrix protein (COMP). COMP-Ang1 is more potent than native Ang1 in phosphorylating the Tie2 receptor and signaling via Akt in primary cultured endothelial cells.[10]

In the present study, we investigated effects of period and dose of COMP-Ang1 on vascular enlargement and tissue blood flow in adult mice and investigated a possible mechanism for long-lasting vascular enlargement induced by long-term and sustained COMP-Ang1. To determine the underly-

Original received March 29, 2005; resubmission received May 10, 2005; revised resubmission received June 8, 2005; accepted June 8, 2005.

From the Biomedical Research Center and Department of Biological Sciences (C.-H.C., K.E.K., G.M.L., G.Y.K), Korea Advanced Institute of Science and Technology, Daejeon, Korea; the Department of Medicine (J.B., H.-S.J., D.-K.K.), Samsung Medical Center and Samsung Biomedical Research Institute, Sungkyunkwan University School of Medicine, Seoul, Korea; the Cardiovascular Research Institute, Comprehensive Cancer Center, and Department of Anatomy (P.B., F.B., D.M.M.), University of California, San Francisco; the Department of Structural Analysis (N.M.), National Cardiovascular Center Research Institute, Suita, Osaka, Japan; the Department of Anatomy (J.K.), College of Medicine, The Catholic University of Korea Seoul; and the Department of Physiology (B.H.J), College of Medicine, Chungnam National University Daejeon, Korea.

Correspondence to Gou Young Koh, Biomedical Research Center, Korea Advanced Institute of Science and Technology, 373-1, Guseong-dong, Daejeon, 305-701, Republic of Korea. E-mail gykoh@kaist.ac.kr

Circulation Research is available at http://circres.ahajournals.org DOI: 10.1161/01.RES.0000174093.64855.a6

ing mechanism of COMP-Ang1–stimulated vascular remodeling in adult mice, we focused on the microvasculature of the trachea, which is distinguished by its simplicity and monolayer structure. Our results indicate that long-term and sustained COMP-Ang1 produced by adenoviral delivery of COMP-Ang1 induces a long-lasting vascular enlargement and enhanced blood flow without enhanced pericyte recruitment in adult mice. Long-lasting Tie2 expression could be involved in the long-lasting vascular enlargement and enhanced blood flow.

Materials and Methods

Generation of COMP-Ang1 Recombinant Protein and Ade-COMP-Ang1

Recombinant Chinese hamster ovary cells expressing COMP-Ang1 (CA1–2; production rate, ≈30 mg/L) were established as previously described.[11] Recombinant adenovirus expressing COMP-Ang1 or LacZ was constructed using the pAdEasy vector system (Qbiogene). For additional Materials and Methods, see online data supplement at http://circres.ahajournals.org.

Animals, Treatment, and Measurement of Blood Pressure and Heart Rate

Specific pathogen-free FVB/N mice and Tie2-GFP transgenic mice (FVB/N)[12] were purchased from Jackson Laboratory and bred in our pathogen-free animal facility. Male mice 8 to 10 weeks old were used for this study. Animal care and experimental procedures were performed under approval from the Animal Care Committees of the Korea Advanced Institute of Science and Technology. For protein treatment, 200 μg of COMP-Ang1 recombinant protein or BSA dissolved in 50 μL of sterile 0.9% NaCl was injected daily through the tail vein for 2 weeks. For adenoviral treatment, the indicated amount of Ade-COMP-Ang1, Ade-LacZ, or Ade-sTie2-Fc (generous gift from Drs Gavin Thurston and Ella Ioffe at Regeneron Pharmaceuticals, Terrytown, NY) diluted in 50 μL of sterile 0.9% NaCl was injected intravenously through the tail vein. Systemic blood pressure and heart rate were measured under anesthesia.

Enzyme-Linked Immunosorbent Assay

Approximately 50 μL of blood was obtained from the tail vein into a heparinized capillary tube at the indicated times. ELISA was adopted for precise detection of COMP-Ang1 in plasma.

Immunohistochemical Staining

Mice were anesthetized, perfused with 1% paraformaldehyde in PBS, and several organs including tracheas were removed. Tracheas and ear skins were immunostained as whole mounts, whereas other organs were immunostained as sections. Signals were visualized, and digital images were obtained with a Zeiss Apotome microscope and a Zeiss LSM 510 confocal microscope.

Measurement of Tracheal Tissue Blood Flow

After the mice were anesthetized, a type N flowprobe (Transonic Systems Inc, Ithaca, NY) was placed on tracheal wall along second, third, and forth cartilage rings without applying pressure, as this would occlude the vessels and reduce perfusion in the area of interest. The flowprobe was kept in place on the position of the highest sensitivity by a micromanipulator and connected to a laser-Doppler flowmeter (model BLF21; Transonic Systems Inc), which can measure microcirculation in 1 mm^3 of tissue for real-time assessment of perfusion (mL/min per 100 g of tissue).

Morphometric Measurements and Statistics

Morphometric measurements of the vessel diameters and area densities in mouse trachea were made as previously described.[13] For each trachea, the numbers of PH3-immunopositive endothelial cells, platelet/endothelial cell adhesion molecule (PECAM)-1–immunopositive blood vessels, and desmin/NG2-immunopositive pericytes were measured in 5 regions, each 0.21 mm^2 in area. Values were expressed per millimeter squared. Values presented are mean±SD. Significance of differences between mean was tested by analysis of variance followed by the Student–Newman–Keuls test. Statistical significance was set at $P<0.05$.

Results

Systemic Adenoviral COMP-Ang1 Produces Differential Enlargements of Blood Vessels in Mouse Tracheal Mucosa

For in vivo treatments with COMP-Ang1, we developed a stable Chinese hamster ovary cell line (CA1–2) which produces COMP-Ang1 at ≈30 mg/L. The potency, solubility, oligomerization status, and stability of the COMP-Ang1 produced from CA1–2 are similar to those of COMP-Ang1 produced from COS-7 cells transiently transfected with plasmid vector containing the COMP-Ang1 gene[10] (data not shown). Adult mice were treated with a daily intravenous injection of 200 μg of COMP-Ang1 recombinant protein or BSA through the tail vein for 2 weeks, then blood vessels in the tracheal mucosa were visualized with PECAM-1 immunostaining (Figure 1). Six segments of the microvasculature were distinguished by their position in the vascular hierarchy and differences in endothelial cell morphology.[14] Enlargement of tracheal blood vessels was found in mice that received COMP-Ang1 in the following descending order of effect: postcapillary venules>capillaries>collecting venules>venules>terminal arterioles (Figure 1B). No significant change was noted in segmental arterioles. These phenomena were observed in all individuals of several mouse strains studied (FVB/N, C57BL/6, BALB/c, BALB/c-*nu*, C3H/HeJ). No changes in the sizes or shape of tracheal blood vessels were found in mice that received BSA.

Short-Term and Intermittent Circulating COMP-Ang1 Induces Reversible Enlargement of Postcapillary Venules and Arterioles in Tracheal Vessels

When 200 μg of COMP-Ang1 recombinant protein was injected intravenously into adult male mice, circulating COMP-Ang1 level peaked immediately after injection (≈3.75 minutes), then declined, and returned almost to the control level 3 to 4 hours after treatment (Figure 2A, left). The half-life ($t_{1/2}$) of circulating COMP-Ang1 was 11.8 minutes. Daily intravenous injection of 200 μg of COMP-Ang1 for 1 week in mice produced an ≈2.0-fold enlargement of postcapillary venules and a 1.4-fold enlargement of terminal arterioles in the trachea (Figure 2). The COMP-Ang1–induced enlargement of postcapillary venules, collecting venules, venous end of capillaries, venules, and terminal arterioles were further increased up to 2 weeks on continuation of daily injection of COMP-Ang1 for up to 2 weeks. However, COMP-Ang1–induced enlarged blood vessels returned gradually to normal after discontinuation of the COMP-Ang1 treatment (Figure 2). One month after discontinuation of the COMP-Ang1 treatment, a second round of treatment with a daily intravenous injection of 200 μg of COMP-Ang1 for 2 weeks induced similar enlargements

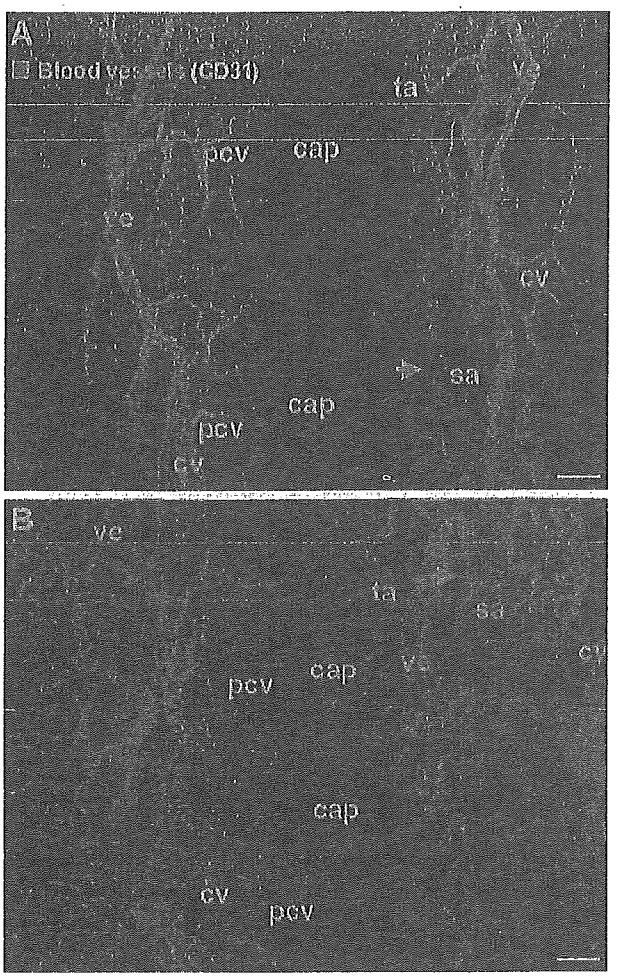

Figure 1. Effect of systemic COMP-Ang1 protein treatment on blood vessels in mouse tracheal mucosa. FVB/N mice were treated with daily injections of 200 μg of BSA (A) or 200 μg of COMP-Ang1 recombinant protein (B) for 14 days. Blood vessels in tracheal whole mounts were visualized with PECAM-1 (CD31) immunostaining (red). Six segments of the microvascular hierarchy are evident: segmental arteriole (sa, arrows), terminal arteriole (ta), capillary (cap), postcapillary venule (pcv), collecting venule (cv), and venule (ve). Of these, postcapillary venules and the venous ends of capillaries were the most enlarged after treatment by COMP-Ang1. The results from 4 experiments were similar. Scale bar=50 μm.

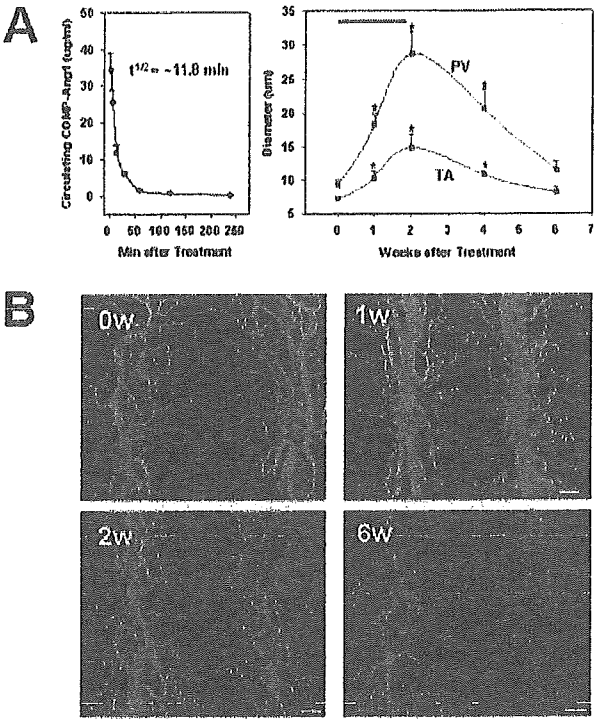

Figure 2. Effect of systemic COMP-Ang1 protein treatment on postcapillary venules and terminal arterioles. FVB/N mice were treated by daily injection of COMP-Ang1 recombinant protein (200 μg) for 14 days (A, black bar). At the indicated times, tracheal vessels were visualized with PECAM-1 immunostaining (B, red). The diameter of postcapillary venules and terminal arterioles are shown (A, right). Circulating plasma levels of COMP-Ang1 were measured by ELISA after a single injection of COMP-Ang1 recombinant protein (200 μg/mouse) (A, left). Diameters of 35 to 40 postcapillary venules (PV)/5 fields (brown curve) and 10 to 12 terminal arterioles (TA)/10 fields (blue curve) were measured at the edge of cartilage rings in each mouse. Values are mean±SD from 4 to 5 mice. *$P<0.05$ vs control period. COMP-Ang1 induced enlargement of postcapillary venules, collecting venules, venous ends of capillaries, venules, and terminal arterioles for up to 2 weeks, and then the enlarged blood vessels returned gradually to normal after discontinuation of the COMP-Ang1 treatment. Scale bar=50 μm.

of tracheal vessels, again in a reversible manner (data not shown). In comparison, the diameters of tracheal vessels were indistinguishable between the control and experimental periods in tracheal vessels of mice treated with BSA (data not shown). These results indicate that short-term spikes of circulating COMP-Ang1 induce reversible enlargement of some tracheal vessels.

Long-Term and Sustained Circulating COMP-Ang1 Induces Long-Lasting Enlargement of Postcapillary Venules and Terminal Arterioles in Tracheal Vessels

As an alternative method for systemic treatment with COMP-Ang1, an adenoviral vector encoding the COMP-Ang1 gene (Ade-COMP-Ang1) was developed. As a control, an adenoviral vector encoding the LacZ gene (Ade-LacZ) was developed. The potency, solubility, oligomerization status, and stability of the COMP-Ang1 produced from HEK293 cells transduced with Ade-COMP-Ang1 are similar to that of COMP-Ang1 produced from COS-7 cells transiently transfected with plasmid vector containing the COMP-Ang1 gene[10] (data not shown). Adult mice were treated with 1×10^9 pfu Ade-COMP-Ang1 or Ade-LacZ. At multiple times more than a period of 16 weeks, circulating plasma COMP-Ang1 levels were measured, and blood vessels in tracheal mucosa were visualized with PECAM-1 immunostaining (Figure 3). Circulating COMP-Ang1 increased as early as 12 hours after treatment, peaked at 1 to 2 weeks, declined gradually thereafter, and returned to control levels at 6 weeks after treatment (Figure 3A). The peak concentrations of circulating COMP-Ang1 were ≈3.5 to 4.5 μg. Significant enlargement of postcapillary venules, capillaries (distinctively, only the venous end of capillaries was enlarged), collecting venules, and terminal arterioles, but not segmental arterioles, was notice-

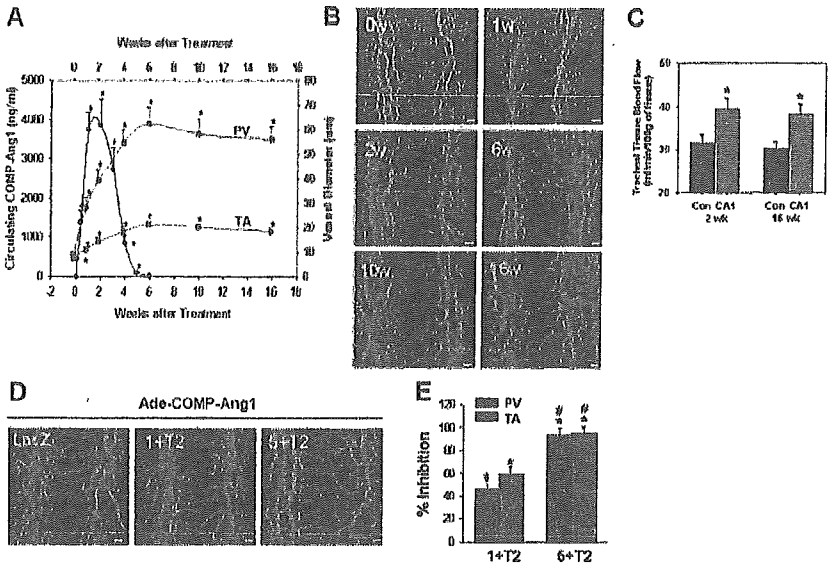

Figure 3. Effect of adenoviral COMP-Ang1 on postcapillary venules and terminal arterioles and blood flow. A through D, FVB/N mice were treated with 1×10^9 pfu Ade-COMP-Ang1 (n=6). At the indicated times, circulating plasma levels of COMP-Ang1 were measured by ELISA (A, black circle), and tracheal vessels were visualized with PECAM-1 immunostaining (B, red). The diameters of postcapillary venules (PV, brown curve) and terminal arterioles (TA, blue curve) are shown. Diameters of 35 to 40 PV/5 fields and 10 to 12 TA/10 fields were measured at the edge of cartilage rings in each mouse. Values are mean±SD from 4 to 5 mice. *P<0.05 vs control period. Scale bar=50 μm. C, Laser-Doppler flowmetric analyses for tracheal tissue blood flows of the mice treated with 1×10^9 pfu Ade-LacZ (Con) or 1×10^9 pfu Ade-COMP-Ang1 (CA1). Quantification of tracheal blood flows at 2 and 16 weeks after treatment with Con or CA1. Bars represent mean±SD from 4 to 5 mice. *P<0.05 vs Con. D and E, FVB/N mice were pretreated with 1×10^8 (1+T2) or 5×10^8 (5+T2) pfu Ade-sTie2-Fc (n=5 each), or 5×10^8 pfu Ade-LacZ (LacZ, n=5) at 24 hours before 1×10^9 pfu Ade-COMP-Ang1 treatment. Two weeks later, tracheal vessels were visualized by PECAM-1 immunostaining (D, red). Scale bar=50 μm. Diameters of 35 to 40 PV/5 fields and 10 to 12 TA/10 fields were measured at the edge of cartilage rings in each mouse. E, Bars represent the mean±SD from 5 experiments as percentage of inhibition of vascular remodeling induced by the pretreatment. Vascular remodeling induced by pretreatment of the Ade-LacZ is arbitrarily given as 100%. *P<0.05 vs LacZ, #P<0.05 vs 1+T2.

able at 1 week after the Ade-COMP-Ang1 treatment (Figure 3B). The vascular enlargements induced by Ade-COMP-Ang1 increased further for up to 6 weeks and then reached a plateau (Figure 3A and 3B). For example, the diameter of postcapillary venules increased 4.3-fold at 2 weeks, 6.0-fold at 4 weeks, and 6.8-fold at 6 weeks (Figure 3A). The enlargement of terminal arterioles was also significant beginning at 1 week after the treatment and increased in a time-dependent manner. However, the increase in diameter in terminal arterioles was less than that in postcapillary venules (Figure 3A and 3B). Importantly, the size of Ade-COMP-Ang1–induced enlarged blood vessels did not significantly decrease for as long as 16 weeks after the treatment, although circulating COMP-Ang1 returned to the control level at 6 weeks after treatment (Figure 3A). In comparison, diameters of tracheal vessels in mice treated with Ade-LacZ were indistinguishable between the control and experimental periods (data not shown). Using a laser-Doppler flowmeter, tracheal tissue blood flows were measured at 2 weeks (the peak level of circulating COMP-Ang1) and 16 weeks (undetectable level of circulating COMP-Ang1) after Ade-LacZ or Ade-COMP-Ang1 treatment. At 2 weeks, tracheal tissue blood flow was increased ≈25% in the mice treated with Ade-COMP-Ang1 compared with the mice treated with Ade-LacZ (Figure 3C and 3D). At 16 weeks, importantly, increased tracheal tissue blood flow by Ade-COMP-Ang1 was not significantly changed (Figure 3C and 3D). These results indicate that long term and sustained circulating COMP-Ang1 treatment induces long-lasting enlargement of tracheal blood vessels with long-lasting enhancement of tissue blood flow in the adult mice.

Tie2 Activation Is Involved in COMP-Ang1–Induced Vascular Remodeling

To determine the involvement of Tie2 activation in COMP-Ang1–induced vascular remodeling, the mice were pretreated with 1×10^8 pfu or 5×10^8 pfu Ade-sTie2-Fc at 24 hours before 1×10^8 pfu Ade-COMP-Ang1 treatment. Two weeks later, the diameters of postcapillary venules and terminal arterioles were measured. Pretreatment with 1×10^8 pfu or 5×10^8 pfu Ade-sTie2-Fc suppressed COMP-Ang1–induced vascular remodeling to the following extent: 46.5±7.7% or 93.5±6.4% in postcapillary venules and 59.7±6.6% or 95.1±5.7% in terminal arterioles, respectively (Figure 3E and 3F). These data indicate that COMP-Ang1–induced vascular remodeling is mainly mediated through Tie2 activation in adult tracheal vessels.

Long-Term and Sustained Circulating COMP-Ang1 Induces Various Vascular Remodeling in Different Organ

Both mice treated with Ade-LacZ (1×10^9 pfu) and those treated with Ade-COMP-Ang1 (1×10^9 pfu) appeared generally healthy, as they gained weight normally. However, the skin of mice treated with Ade-COMP-Ang1 appeared strikingly redder than the skin of mice treated with Ade-LacZ, beginning 10 to 14 days after the treatment. The Ade-COMP-

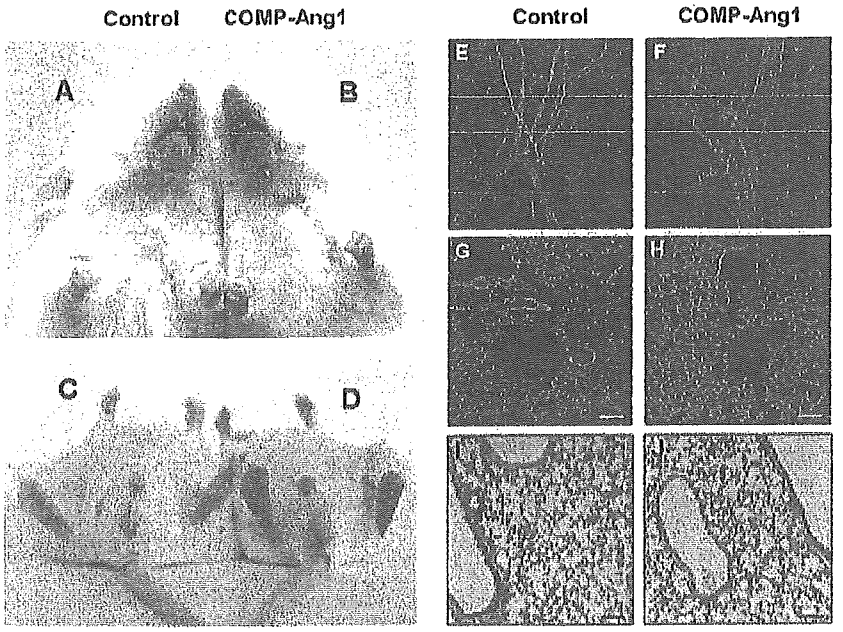

Figure 4. Effect of adenoviral COMP-Ang1 on skin color and vascular remodeling in ear skin and lung at 16 weeks after treatment. FVB/n mice were treated with 1×10^9 pfu Ade-LacZ or Ade-COMP-Ang1. Sixteen weeks later, the skin color of the face, hands, soles, penis, and tail were photographed (A, B, C, and B), blood vessels in ear skin (E and F) and lungs (G and H) were visualized with PECAM-1 (CD31) immunostaining (red), and sections of lungs were stained with H&E (I and J). The mice treated with Ade-COMP-Ang1 show overt skin redness, have prominently enlarged blood vessels in the ear skin, and have more dense PECAM-1–positive endothelial cells in the lung without overt histologic alteration compared with the mice treated with Ade-LacZ. The results from 4 experiments were similar. Scale bar = 50 μm.

Ang1–induced skin redness persisted for as long as 16 weeks after the treatment (Figure 4). Sixteen weeks after the treatment, skin color in hair-sparse portions such as the face, hands, soles, penis, and tail of mice treated with Ade-COMP-Ang1 were distinctly redder than those of mice treated with Ade-LacZ. Blood vessels of the ear and capillaries of the heart, adrenal cortex, and liver of the mice treated with Ade-COMP-Ang1 were enlarged (Figures 4 and 5). More PECAM-1–positive endothelial cells were present in the lung, heart, liver, and renal medulla of mice treated with Ade-COMP-Ang1 compared with the mice treated with Ade-LacZ (Figures 4 and 5 and online Figure I in the data supplement). However, blood vessels of the renal cortex, including glomeruli, and intestinal villi of the mice treated with Ade-COMP-Ang1 and the mice treated with Ade-LacZ were indistinguishable. In addition, the body weights, systemic blood pressures, and heart rates of the 2 groups of mice were indistinguishable. These results indicate that long-term and sustained circulating COMP-Ang1 treatment induces long-lasting tissue-specific vascular remodeling in different blood vessels without notable changes in systemic blood pressure and heart rate (online Table I).

Induction of Tie2 Could Be Involved in Permanent Changes of COMP-Ang1–Induced Vascular Remodeling

Based on these observations, we asked whether Tie2 expression was more abundant in postcapillary venules than termi-

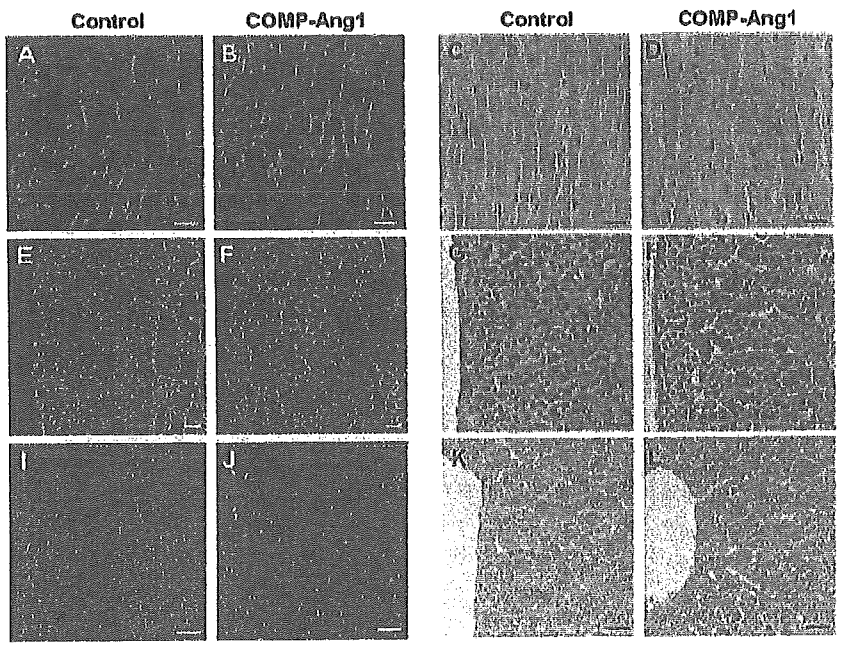

Figure 5. Effect of adenoviral COMP-Ang1 on vascular remodeling in heart, adrenal cortex, and liver at 16 weeks after the treatment. FVB/n mice were treated with 1×10^9 pfu Ade-LacZ or Ade-COMP-Ang1. Sixteen weeks later, blood vessels in heart (A through D), adrenal cortex (E through H), and liver (I through L) were visualized with PECAM-1 (CD31) immunostaining (red), and the sections were stained with H&E. The mice treated with Ade-COMP-Ang1 have enlarged capillaries in the heart and adrenal cortex and more PECAM-1–positive endothelial cells in the liver compared with the mice treated with Ade-LacZ. The results from 4 experiments were similar. Scale bar = 25 μm.

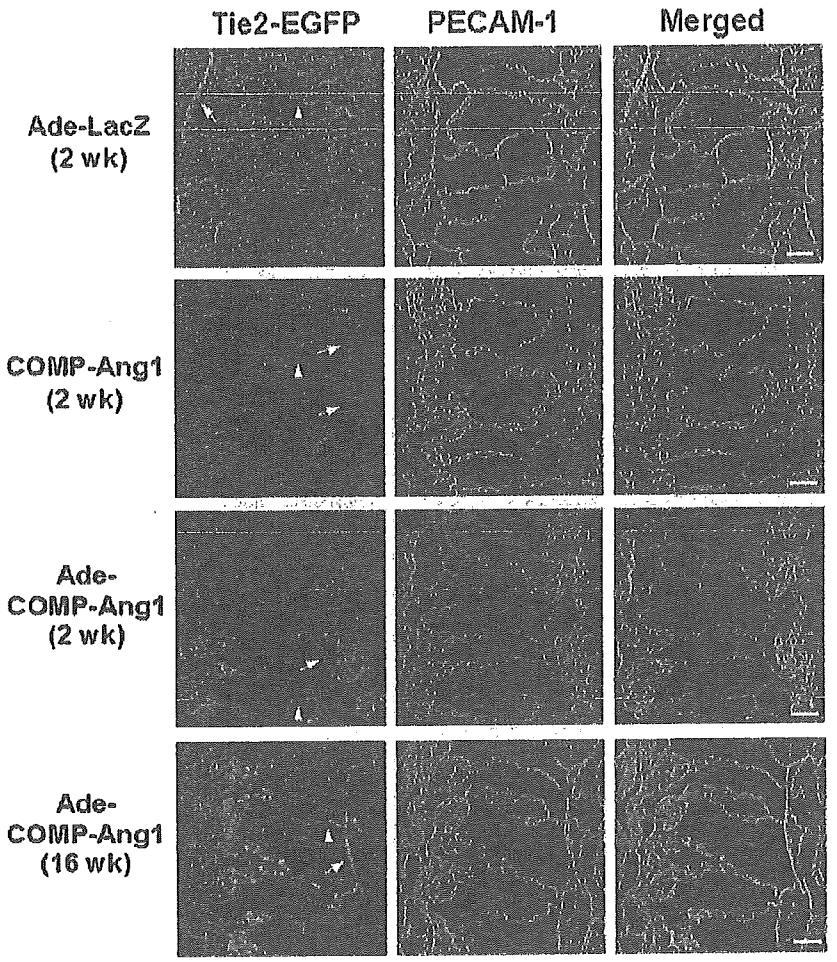

Figure 6. Induction of Tie2 expression in COMP-Ang1–induced vascular remodeling. Tie2-GFP transgenic mice (10 weeks old) were treated with daily injection of 200 μg of COMP-Ang1 recombinant protein (COMP-Ang1) for 2 weeks or a single injection of 1×10^9 pfu Ade-LacZ or Ade-COMP-Ang1. At 2 and 16 weeks after the beginning of the treatments, Tie2 expression in tracheal vessels was visualized by GFP expression (green) and PECAM-1 immunostaining (red), and the images were merged. The results from 4 experiments were similar. Arrowhead indicates terminal arterioles; arrow, precapillary arterioles. Scale bar=50 μm.

nal arterioles in mouse trachea. Therefore, we examined the extent of Tie2 expression using transgenic mice with Tie2 promoter–driven green fluorescent protein (GFP).[12] In the tracheal mucosa of adult mice, Tie2 expression was not detectable in most endothelial cells of postcapillary venules, whereas it was moderately expressed in endothelial cells of terminal and precapillary arterioles of tracheal vessels (Figure 6). Thus, differential enlargement of tracheal vessels on COMP-Ang1 stimulation is not dependent on the extent of Tie2 expression. However, Tie2 expression was markedly increased in endothelial cells of collecting venules, venules, postcapillary venules, and capillaries at 2 weeks after the Ade-COMP-Ang1 treatment (Figure 6), which is somewhat consistent with a recent report with Ade-Ang1.[8] Tie2 expression was further increased in endothelial cells of the same vessels at 16 weeks after the Ade-COMP-Ang1 treatment (Figure 6). In contrast, Tie2 expression was not changed in any endothelial cells of enlarged tracheal vessels at 2 weeks after the recombinant COMP-Ang1 protein treatment (Figure 6). Area densities of Tie2 expression in a given microscopic field area (0.22 mm^2) for arterioles, capillaries, and venules in tracheal mucosa were 8.2±1.7, 2.8±0.4, and 3.3±0.6% (mean±SD from 4 mice), respectively, after Ade-LacZ treatment (at 2 weeks); 7.6±1.9, 3.1±0.5, and 3.7±0.6% after COMP-Ang1 protein treatment (at 2 weeks); 11.3±2.2, 10.3±1.7, and 28.1±5.4% after Ade-COMP treatment (at 2 weeks); and 13.3±2.7, 18.2±3.5, and 47.7±7.2 after Ade-COMP treatment (at 16 weeks). In addition, Tie2 expression was notably higher in the enlarged veins of abdominal skin and the sinusoidal capillaries in liver of the mice treated with Ade-COMP-Ang1 than the mice treated with Ade-LacZ at 16 weeks after the treatment (online Figure II). Thus, Tie2 expression in venular and capillary endothelial cells could be induced with long-term and sustained Tie2 stimulation induced by Ade-COMP-Ang1 but not with short-term spiked Tie2 stimulation induced by recombinant COMP-Ang1 protein.

COMP-Ang1–Induced Vascular Enlargement Could Result From Circumferential Endothelial Cell Proliferation

COMP-Ang1–induced enlargement of blood venules appears to result from endothelial cell proliferation rather than vasodilation or endothelial cell hypertrophy because the endothelial cells were normal in size (Figure 7A and 7B). To test this possibility, we examined by immunostaining the number of endothelial cells positive for phosphohistone H3 (nuclear protein of diving cell). Numerous phosphohistone H3–positive immunostained endothelial cells were detected in various portions including postcapillary venules, capillaries, collect-

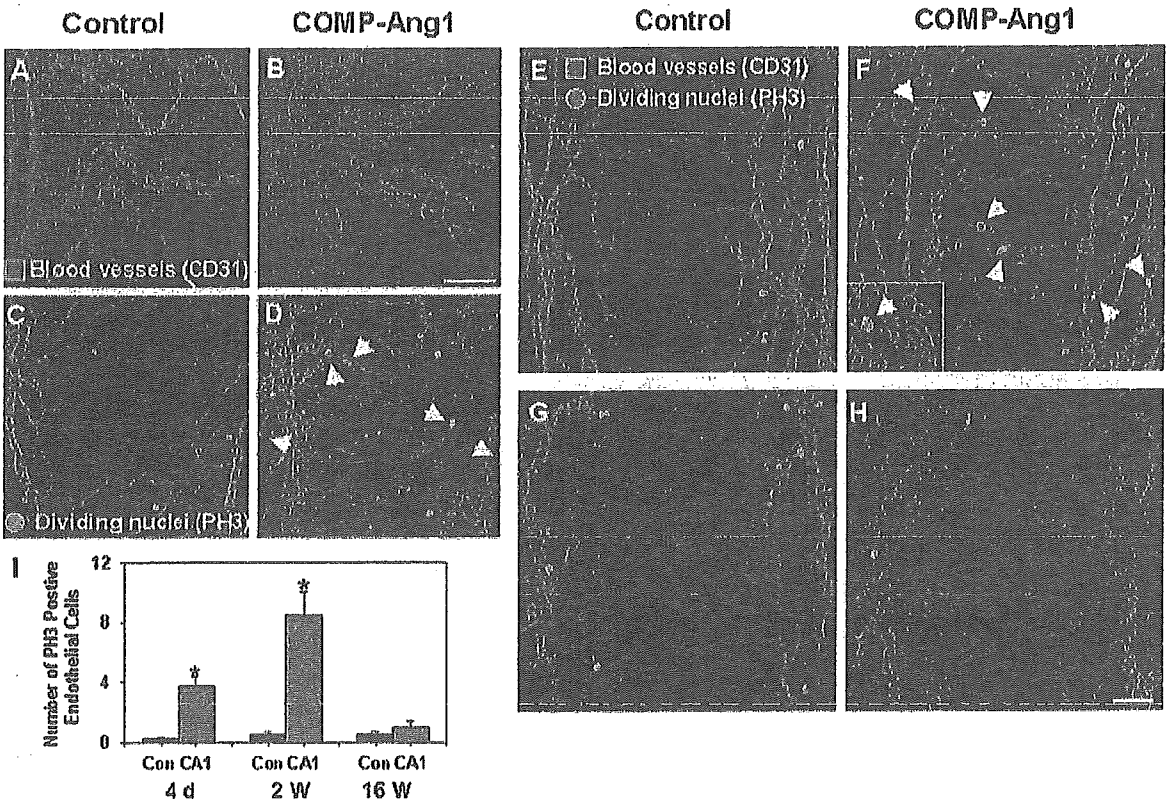

Figure 7. Increased number of dividing endothelial cells during COMP-Ang1–induced enlargement. FVB/N mice were treated with 1×10^9 pfu Ade-LacZ (control; A, C, E, and G) or Ade-COMP-Ang1 (COMP-Ang1; B, D, F, and H). Four days (C and D), 2 weeks (E and F), and 16 weeks (G and H) later, tracheal vessels were visualized with PECAM-1 (CD31) immunostaining (red) and phosphohistone H3 (PH3) immunostaining (green). F, Arrow indicates PH3-immunopositive endothelial cells; white square, PH3-immunopositive endothelial cells in postcapillary venule at higher magnification. Scale bar=50 μm. I, Number of PH3-immunopositive endothelial cells in a given 0.21 mm^2 area. Bars represent mean±SD from 4 mice. Con indicates control; CA1, COMP-Ang1. *$P<0.05$ vs Con.

ing venules, venules, and terminal arterioles of tracheal vessels at 4 days and 2 weeks after the Ade-COMP-Ang1 treatment (Figure 7D, 7F, and 7I) or after recombinant COMP-Ang1 protein treatment (data not shown). However, almost no phosphohistone H3–positive endothelial cells were detected in any portion of tracheal vessels at 4 days or 2 and 16 weeks after the Ade-LacZ treatment and at 16 weeks after the Ade-COMP-Ang1 treatment (Figure 7C, 7E, 7G, and 7I). These findings indicate that vascular enlargement induced by COMP-Ang1 is more likely to result from endothelial cell proliferation depending on concentration of circulating COMP-Ang1 than from vasodilation or endothelial cell hypertrophy.

COMP-Ang1–Induced Postcapillary Venule Enlargement Is Not Accompanied by Pericyte Recruitment

Ang1 is known to be a strong growth factor for pericyte recruitment to nascent endothelial cells during vasculogenesis in physiological and pathological conditions.[3–5] Therefore, we examined the interaction between endothelial cells and pericytes in the enlarged blood vessels of the trachea by double-immunostaining for endothelial cells and pericytes at 4 weeks after Ade-LacZ or Ade-COMP-Ang1 treatment. The interaction of endothelial cells and pericytes in most of tracheal blood vessels (except postcapillary venules) in mice that received Ade-COMP-Ang1 was similar to that in mice that received Ade-LacZ (Figure 8). Although less interaction of endothelial cells with pericytes was found on the enlarged postcapillary venules than elsewhere, the number of pericytes of the enlarged postcapillary venules was similar to the control postcapillary venules (Figure 8). Thus, COMP-Ang1 did not promote pericyte recruitment to the COMP-Ang1–induced enlarged venules in the trachea.

Discussion

The most important and novel finding in this study is that enlargement of tracheal blood vessels and enhancement of tracheal tissue blood flow induced by long-term and sustained exposure to COMP-Ang1 had not regressed for up to 16 weeks, despite the fact that exposure to COMP-Ang1 had already been discontinued at 6 to 7 weeks in adult mice. In comparison, enlargement of tracheal blood vessels induced by short-term intermittent exposure to COMP-Ang1 regressed on discontinuation of recombinant COMP-Ang1 treatment. Therefore, long-lasting vascular enlargement and enhancement of blood flow can be achieved by long-term and sustained exposure to COMP-Ang1.

Like other therapeutic proteins, circulating COMP-Ang1 rapidly disappeared in the plasma, probably because of its trapping by the Tie2 receptor of lung endothelial cells.[15]

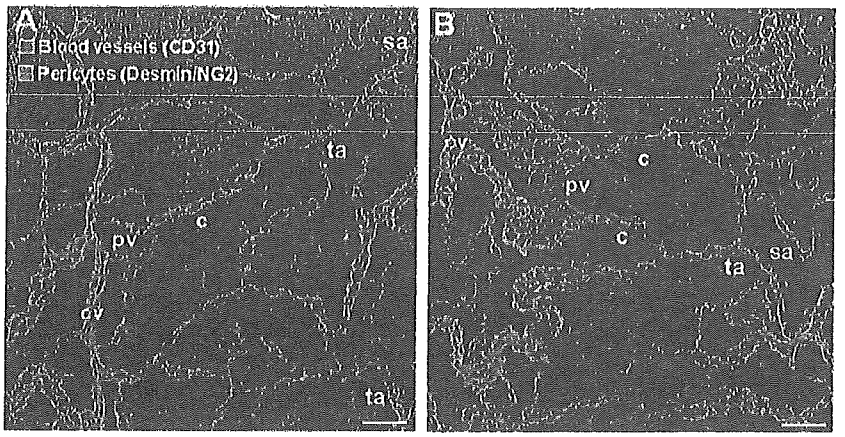

Figure 8. Interaction between endothelial cells and pericytes in COMP-Ang1–induced enlarged tracheal vessels. FVB/n mice were treated with 1×10^9 pfu Ade-COMP-Ang1 (B) or Ade-LacZ (A). Four weeks later, tracheal vessels were visualized with PECAM-1 (CD31) immunostaining (red), and pericytes were visualized with desmin/NG2 immunostaining (green). The results from 4 experiments were similar. Scale bar=50 μm.

However, we were able to achieve long-term (>4 weeks) and sustained (>1000 ng/mL) circulating COMP-Ang1 in mice by a single intravenous injection of 1×10^9 pfu Ade-COMP-Ang1. Throughout these experiments, we learned that long-term (≈6 weeks) and sustained exposure to COMP-Ang1 produced long-lasting enlargement of postcapillary venules and terminal arterioles in the tracheal mucosa, whereas short-term (≈2 weeks) and intermittent exposure to COMP-Ang1 produced reversible enlargements of these vessels. Similar to our results, another study found that long-term (4 weeks) sustained exposure to vascular endothelial growth factor (VEGF) produced long-lasting acquired vascular remodeling in liver, whereas short-term (2 weeks) sustained exposure to VEGF produced reversible vascular remodeling.[16] What are the major mechanisms and factors that produce long-lasting and reversible vascular remodeling? Is there a threshold stimulation of Tie2 by COMP-Ang1 that can produce permanent enlargement? Our results suggest that auto-amplification of Tie2 expression by treatment with COMP-Ang1 above a certain dose and exposure period could be one of the mechanisms. Once Tie2 expression is activated by a long-term and excess exposure to COMP-Ang1, after discontinuation of COMP-Ang1, the subsequent activation of Tie2 might be achieved by endogenous circulating Ang1 or increased shear stress caused by increased blood flow.[17] However, auto-amplification of Tie2 expression cannot be achieved below a certain dose and exposure period of COMP-Ang1, as evidenced by the experiments with intravenous administration of COMP-Ang1 recombinant protein. Therefore, the dose and the exposure period of COMP-Ang1 or VEGF should be considered in any therapeutic approaches where permanent vascular enlargements are needed to alleviate dysfunctions of ischemic tissues.

Tie1, an endothelial-specific receptor tyrosine kinase, shares a high degree of homology with Tie2. Although Tie1 was isolated more than a decade ago,[18] no ligand had been found to activate it. Recently, Saharinen et al demonstrated that COMP-Ang1 stimulated Tie1 phosphorylation in cultured endothelial cells.[19] Moreover, they showed that COMP-Ang1–induced Tie1 activation was amplified via Tie2 and was more efficient than native Ang1- and Ang4-induced Tie1 activation. Thus, COMP-Ang1 and Ang1 are now known to be activating ligands for both Tie1 and Tie2. However, our data indicate that COMP-Ang1–induced vascular remodeling in adult tracheal vessels is mainly mediated through activation of Tie2, not by Tie1. (See expanded Discussion section in the online data supplement.)

Although Ang1 induces vascular enlargement and has therapeutic benefits to ischemic tissues in several experimental animal models,[6,7,9] little is known about whether the vascular enlargement is accompanied by enhanced blood flow. Our results showed that COMP-Ang1–induced vascular enlargement was accompanied by enhanced tissue blood flow in the trachea. Therefore, enhanced blood flow through arteriolar and venular enlargements induced by COMP-Ang1 could provide a great therapeutic benefit to ischemic peripheral tissues. In fact, Ang1-induced vessel enlargement is a unique characteristic among many growth factors. Our immunohistological examination of phosphohistone H3 revealed that COMP-Ang1–induced vascular enlargements were evidently the result of endothelial proliferation, which is consistent with a recent report.[14] Thus, arteriolar and venular enlargements are achieved mainly by circumferential endothelial proliferation, which is a unique phenomenon and is different from multidirectional endothelial cell proliferation during vasculogenesis and angiogenesis. Moreover, our results revealed that different organs showed different sensitivities to long-term and sustained COMP-Ang1. In fact, blood vessels in the skin, heart, adrenal cortex, and liver, among other organs, are relatively sensitive to the COMP-Ang1–induced vascular enlargement. Therefore, COMP-Ang1 could provide a great therapeutic benefit to patients with delayed skin wound healing and ischemic heart diseases through its ability to promote vascular remodeling. Nevertheless, the mice treated with long-lasting and sustained COMP-Ang1 did not show any significant changes in body weight, systemic blood pressure, or heart rate. More detailed analysis will be necessary to clarify how it is possible that the mice with enlarged blood vessels caused by long-term and sustained COMP-Ang1 have normal blood pressure and heart rate.

Ang1 is known to be a strong growth factor for pericyte recruitment to nascent endothelial cells during development.[3–5] This Ang1-induced pericyte recruitment is related to the Ang1-induced antileakage effect on VEGF and proinflammatory stimuli.[5] However, our results show a lower number and poorer covering of pericytes in COMP-Ang1–

induced enlarged postcapillary venules. In fact, in a mouse model that completely blocks pericyte recruitment to developing vessels by injection of antagonistic monoclonal antibody against platelet-derived growth factor receptor-β, Angl is able to restore a hierarchical architecture of growing blood vessels and rescues retinal edema and hemorrhage even in the absence of pericyte recruitment.[20] Thus, COMP-Angl may be able to assemble endothelial cells in a frame of hierarchical architecture without pericyte recruitment in the COMP-Angl–induced enlarged blood vessels.

In conclusion, long-lasting vascular enlargement and enhancement of blood flow can be achieved by long-term and sustained exposure to COMP-Angl.

Acknowledgments

Supported, in part, by the Bio-Challenge Program and the National Research Laboratory Program (2004-02376 to G.Y.K.) of the Korean Ministry of Science and Technology, the Korea Health R&D Project (0405-DB01-0104-0006 to G.Y.K.), the Ministry of Health & Welfare, and the Korea Science and Engineering Foundation (R01-2004-000-10045-0 to B.H.J.). Also supported by National Institutes of Health grants HL-24136 and HL-59157 from the National Heart, Lung and Blood Institute (to D.M.D.).

References

1. Davis S, Aldrich TH, Jones PF, Acheson A, Compton DL, Jain V, Ryan TE, Bruno J, Radziejewski C, Maisonpierre PC, Yancopoulos GD. Isolation of angiopoietin-1, a ligand for the TIE2 receptor by secretion-trap expression cloning. *Cell*. 1996;87:1161–1169.
2. Dumont DJ, Gradwohl G, Fong GH, Puri MC, Gertsenstein M, Auerbach A, Breitman ML. Dominant-negative and targeted null mutations in the endothelial receptor tyrosine kinase, tek, reveal a critical role in vasculogenesis of the embryo. *Genes Dev*. 1994;8:1897–1909.
3. Suri C, Jones PF, Patan S, Bartunkova S, Maisonpierre PC, Davis S, Sato TN, Yancopoulos GD. Requisite role of angiopoietin-1, a ligand for the TIE2 receptor, during embryonic angiogenesis. *Cell*. 1996;87:1171–1180.
4. Suri C, McClain J, Thurston G, McDonald DM, Zhou H, Oldmixon EH, Sato TN, Yancopoulos GD. Increased vascularization in mice overexpressing angiopoietin-1. *Science*. 1998;282:468–471.
5. Thurston G, Suri C, Smith K, McClain J, Sato TN, Yancopoulos GD, McDonald DM. Leakage-resistant blood vessels in mice transgenically overexpressing angiopoietin-1. *Science*. 1999;286:2511–2514.
6. Shyu KG, Manor O, Magner M, Yancopoulos GD, Isner JM. Direct intramuscular injection of plasmid DNA encoding angiopoietin-1 but not angiopoietin-2 augments revascularization in the rabbit ischemic hindlimb. *Circulation*. 1998;98:2081–2087.
7. Chae JK, Kim J, Lim ST, Chung MJ, Kim WH, Kim HG, Ko JK, Koh GY. Co-administration of angiopoietin-1 and vascular endothelial growth factor enhances collateral vascularization. *Arterioscler Thromb Vasc Biol*. 2000;20:2573–2578.
8. Baffert F, Thurston G, Rochon-Duck M, Le T, Brekken R, McDonald DM. Age-related changes in vascular endothelial growth factor dependency and angiopoietin-1-induced plasticity of adult blood vessels. *Circ Res*. 2004;94:984–992.
9. Zhou YF, Stabile E, Walker J, Shou M, Baffour R, Yu Z, Rott D, Yancopoulos GD, Rudge JS, Epstein SE. Effects of gene delivery on collateral development in chronic hypoperfusion: diverse effects of angiopoietin-1 versus vascular endothelial growth factor. *J Am Coll Cardiol*. 2004;44:897–903.
10. Cho CH, Kammerer RA, Lee HJ, Steinmetz MO, Ryu YS, Lee SH, Yasunaga K, Kim KT, Kim I, Choi HH, Kim W, Kim SH, Park SK, Lee GH, Koh GY. COMP-Angl: a designed angiopoietin-1 variant with nonleaky angiogenic activity. *Proc Natl Acad Sci USA*. 2004;101:5547–5552.
11. Hwang SJ, Choi HH, Kim KT, Hong HJ, Koh GY, Lee GM. Expression and purification of recombinant human angiopoietin-2 produced in CHO cells. *Protein Express Purif*. 2005;39:175–183.
12. Schlaeger TM, Bartunkova S, Lawitts JA, Teichmann G, Risau W, Deutsch U, Sato TN. Uniform vascular-endothelial-cell-specific gene expression in both embryonic and adult transgenic mice. *Proc Natl Acad Sci USA*. 1997;94:3058–3063.
13. Baluk P, Raymond WW, Ator E, Coussens LM, McDonald DM, Caughey GH. Matrix metalloproteinase-2 and -9 expression increases in Mycoplasma-infected airways but is not required for microvascular remodeling. *Am J Physiol Lung Cell Mol Physiol*. 2004;287:L307–L317.
14. McDonald DM. Endothelial gaps and permeability of venules in rat tracheas exposed to inflammatory stimuli. *Am J Physiol*. 1994;266:L61–L83.
15. Cho CH, Kammerer RA, Lee HJ, Yasunaga K, Kim KT, Choi HH, Kim W, Kim SH, Park SK, Lee GM. A designed angiopoietin-1 variant, COMP-Angl, protects against radiation-induced endothelial cell apoptosis. *Proc Natl Acad Sci USA*. 2004;101:5553–5558.
16. Dor Y, Djonov V, Abramovitch R, Itin A, Fishman GI, Carmeliet P, Goelman G, Keshet E. Conditional switching of VEGF provides new insights into adult neovascularization and pro-angiogenic therapy. *EMBO J*. 2002;21:1939–1947.
17. Lee HJ, Koh GY. Shear stress activates Tie2 receptor tyrosine kinase in human endothelial cells. *Biochem Biophys Res Commun*. 2003;304:399–404.
18. Partanen J, Armstrong E, Makela TP, Korhonen J, Sandberg M, Renkonen R, Knuutila S, Huebner K, Alitalo K. A novel endothelial cell surface receptor tyrosine kinase with extracellular epidermal growth factor homology domains. *Mol Cell Biol*. 1992;12:1698–1707.
19. Saharinen P, Kerkela K, Ekman N, Marron M, Brindle N, Lee GM, Augustin H, Koh GY, Alitalo K. Multiple angiopoietin recombinant proteins activate the Tie1 receptor tyrosine kinase and promote its interaction with Tie2. *J Cell Biol*. 2005;169:239–243.
20. Uemura A, Ogawa M, Hirashima M, Fujiwara T, Koyama S, Takagi H, Honda Y, Wiegand SJ, Yancopoulos GD, Nishikawa S. Recombinant angiopoietin-1 restores higher-order architecture of growing blood vessels in mice in the absence of mural cells. *J Clin Invest*. 2002;110:1619–1628.

THE JOURNAL OF BIOLOGICAL CHEMISTRY
Vol. 280, No. 6, Issue of February 11, pp. 5022–5031, 2005
Printed in U.S.A.

Local Activation of Rap1 Contributes to Directional Vascular Endothelial Cell Migration Accompanied by Extension of Microtubules on Which RAPL, a Rap1-associating Molecule, Localizes*[S]

Received for publication, August 24, 2004, and in revised form, November 23, 2004
Published, JBC Papers in Press, November 29, 2004, DOI 10.1074/jbc.M409701200

Hisakazu Fujita, Shigetomo Fukuhara, Atsuko Sakurai, Akiko Yamagishi, Yuji Kamioka, Yoshikazu Nakaoka, Michitaka Masuda, and Naoki Mochizuki‡

From the Department of Structural Analysis, National Cardiovascular Center Research Institute, Suita, Osaka 565-8565, Japan

Endothelial cell migration is promoted by chemoattractants and is accompanied with microtubule extension toward the leading edge. Cytoskeletal microtubules polarize to function as rails for delivering a variety of molecules by motor proteins during cell migration. It remains, however, unclear how directional migration with polarized extension of microtubules is regulated. Here we report that Rap1 controls the migration of vascular endothelial cells. We found that Rap1-associating molecule, RAPL, which belongs to the Ras association domain family (Rassf), localized on microtubules and that activated Rap1 induced dissociation of RAPL from microtubules. A Rap1 activation-monitoring probe based on the fluorescence resonance energy transfer enabled us to demonstrate that local Rap1 activation occurs at the leading edge of the cells under the two types of cell migration, chemotaxis and wound healing. Time lapse imaging of microtubules marked by enhanced green fluorescent protein-RAPL showed the directional growth of microtubules toward the leading edge of the migrating cells. Using adenovirus, inactivation of Rap1 by expression of rap1GAPII inhibited wound healing. In addition, disconnection of Rap1 and RAPL by expression of a RAPL mutant also perturbed wound healing. Collectively, the locally activated Rap1 and its association with RAPL controls the directional migration of vascular endothelial cells.

Rap1 belongs to the Ras GTPase family and cycles between a GDP-bound inactive form and a GTP-bound active form (1). Rap1 activation is regulated by guanine nucleotide exchange factor (GEF),[1] whereas Rap1 inactivation is regulated by GTPase-activating protein (GAP). GEFs contain a catalytic domain and regulatory domains that either bind to upstream molecules or are regulated by second messengers such as cAMP and Ca^{2+}. The former GEFs include C3G and PDZ-GEF; the latter includes CalDAG-GEFs and Epac (cAMP-GEF) (reviewed in Ref. 2). Thus, the spatial Rap1 activation depends on the localization of GEF and the spreading of second messengers. Like GEFs, the spatial Rap1 inactivation depends on the localization of GAPs for Rap1 (3). We have currently developed a spatio-temporal activation/inactivation monitoring probe for Rap1 in living cells (4).

Once activated by GEFs, GTP-bound Rap1 associates with effector molecules including Raf-1, B-Raf, RalGDS, and AF-6 (2). Rap1 shares these effector molecules with Ras protein; therefore, Rap1 is suggested to function antagonistically on the Ras-activated intracellular signaling pathway. However, Rap1 may have a unique function in regulating cell adhesion (5, 6). Rap1 was recently reported to be indispensable for cell-extracellular matrix (ECM) contacts by stabilizing the cell-ECM contacts, indicating that Rap1 enhances cell adhesion to ECM (7, 8). Moreover, Bud1, the yeast homologue of Rap1, determines the budding site (9), and Rap1 regulates adherens junction positioning for cell division in *Drosophila* (10), implying that Rap1 is also involved in cell polarization.

Cells have a polarity determined by cell protrusions and retractions, when moving toward certain chemoattractants or during wound healing. In the protrusions, actin is actively polymerized and depolymerized, whereas in retractions stabilized actin fibers are observed (11). For perpetual moving toward the chemoattractants, asymmetrical polarity of cell contacts to ECM is required. Focal adhesions connecting actin stress fibers are assembled in the protrusions and disassembled in the retractions of migrating cells (reviewed in Ref. 12). Like actin, microtubules are assembled toward the leading edge of the protrusions. By constituting rails for motor proteins carrying the molecules to the protrusive part of the cell, microtubule promotes cell polarity (13). Furthermore, recently, assembly and disassembly of focal adhesions are reportedly regulated by microtubules (14, 15). Thus, microtubule extension toward the leading edge parallels the change in polarity of the motile cells toward the chemoattractants or during wound healing.

* This work was supported by grants from the Ministry of Health, Labor, and Welfare of Japan; from the Promotion of Fundamental Studies in Health Science of the Organization for Pharmaceutical Safety and Research of Japan; from the Ministry of Education, Science, Sports and Culture of Japan; from the Cell Science Research Foundation; and from the Mochida Memorial Foundation for Medical and Pharmaceutical Research. The costs of publication of this article were defrayed in part by the payment of page charges. This article must therefore be hereby marked "*advertisement*" in accordance with 18 U.S.C. Section 1734 solely to indicate this fact.

[S] The on-line version of this article (available at http://www.jbc.org) contains two additional figures and eight videos.

‡ To whom correspondence should be addressed: Dept. of Structural Analysis, National Cardiovascular Center Research Institute, 5-7-1 Fujishirodai, Suita, Osaka 565-8565, Japan. Tel.: 81-6-6833-5012 (ext. 2508); Fax: 81-6-6835-5461; E-mail: nmochizu@ri.ncvc.go.jp.

[1] The abbreviations used are: GEF, guanine nucleotide exchange factor; CFP, cyan fluorescent protein; ECM, extracellular matrix; EGFP, enhanced green fluorescent protein; FRET, fluorescence resonance energy transfer; GAP, GTPase-activating protein; GFP, green fluorescent protein; GST, glutathione *S*-transferase; HAEC, human aortic endothelial cell; HUVEC, human umbilical vein endothelial cell; MTOC, microtubule-organizing center; Rassf, Ras association domain family; S1P, sphingosine 1-phosphate; SDF-1, stromal-derived factor-1; YFP, yellow fluorescent protein; MES, 4-morpholineethanesulfonic acid.

RAPL/NORE1B (hereafter referred to as RAPL) is identified as a Rap1-binding molecule (16), which contains a Ras/Rap1 binding domain and belongs to the Ras association domain family (Rassf) (17, 18). Whereas Rassf members function as potent suppressors of tumors (19–21), RAPL links Rap1 activation upon T cell receptor cross-linking and stromal-derived factor-1 (SDF-1) stimulation to integrin activation. In addition, RAPL mediates the polarized distribution of SDF-1 receptors upon Rap1 activation (16). Recently, Rassf1 has been shown to localize at and stabilize microtubules (22). However, it is unclear whether other molecules belonging to Rassf function in the association with Ras family GTPases.

We investigate the localization of RAPL in the vascular endothelial cells and how Rap1-RAPL participates in determining the directional migration in response to a chemoattractant, sphingosine 1-phosphate (S1P) (23), and during wound healing. RAPL localizes at the microtubule-organizing center (MTOC) and microtubules. Rap1 is activated at the leading edge of migrating cells. In addition, inactivation of Rap1-RAPL signal perturbed the wound closure. These data suggest that local activation of Rap1 and its association with RAPL regulates the directional cell migration of vascular endothelial cells.

EXPERIMENTAL PROCEDURES

Reagents and Antibodies—S1P was purchased from Biomol (Plymouth, PA). Protein A-Sepharose was from Calbiochem. Anti-green fluorescent protein (GFP) was developed in our laboratory. Anti-β-tubulin, anti-γ-tubulin, and anti-FLAG (M2) were purchased from Sigma, and anti-Rap1 was from BD Biosciences. Anti-RAPL antibody was a kind gift from T. Kinashi (Kyoto University, Japan).

Plasmids—The coding sequences of human Rassf1A, Rassf1C, Rassf2 (KIAA0168), Rassf3, and RAPL (NORE1B) were amplified by PCR using human heart cDNA library as a template. pCA-EGFP-Rassf1A, -Rassf1C, -Rassf2, -Rassf3, and RAPL were derived from pCAGGS eukaryotic expression vector and expressed enhanced green fluorescent protein (EGFP)-tagged each Rassf molecules (24). cDNAs encoding RAPL deletion mutants as indicated in Fig. 4 were amplified by PCR and ligated into pCA-EGFP vector similarly to Rassf1. dC1, dC2, dC3, and dN encoded amino acids 1–222, 1–168, 1–100, and 101–265 of RPAL, respectively. A mutant of RAPL (hereafter referred to as the RA mutant), in which Lys^{123}, Arg^{124}, Lys^{135}, Lys^{154}, Lys^{155}, Asp^{160}, and Asn^{161} were replaced with Ala, was reported to be incapable of associating with Rap1 (16). cDNA encoding an RA mutant was amplified by PCR-based mutagenesis and subcloned into pCA-EGFP. pCXN2-FLAG-Rap1 expressed FLAG-tagged Rap1. Either constitutive active or dominant negative forms of Rap1 (Rap1V12 or Rap1N17) cDNAs were similarly inserted into pCXN2-FLAG. pIRM21-Rap1V12 expressed FLAG-tagged Rap1V12 and internal ribosomal entry site-driven dsFP593 as described previously (24). pIRM21-rap1GAPII expressed both FLAG-tagged rap1GAPII and internal ribosomal entry site-driven dsFP593. pCA-DsRed-CrkI was derived from pCAGGS eukaryotic expression vector as described previously (24). pRaichu-Rap1, a Rap1 activation monitoring probe based on fluorescence resonance energy transfer (FRET), was described previously (4). pRaichu-Rap1 expressed a chimeric protein consisting of yellow fluorescent protein (YFP), Rap1, and Ras-binding domain of Raf and cyan fluorescent protein (CFP) followed by the CAAX motif of Ki-Ras. In pRaichu-Rap1N17, a cDNA encoding Rap1N17 was replaced with that encoding Rap1. pGEX-RAPL was constructed by inserting a cDNA encoding full-length RAPL into pGEX (Amersham Biosciences).

Adenovirus—Both an adenovirus-expressing EGFP-tagged RAPL and an adenovirus-expressing EGFP-tagged RA mutant of RAPL were produced using the Adeno-X expression system (BD Biosciences). Briefly, cDNA from pCA-EGFP-RAPL was inserted into Adeno-X viral DNA using pShuttle as a transfer vector. Adenovirus-expressing EGFP-RAPL was produced from HEK293 cells transfected with Adeno-X-EGFP-RAPL. An adenovirus-expressing RA mutant of RAPL was produced in a similar manner to RAPL-expressing adenovirus. The EGFP-expressing adenovirus and the rap1GAPII-expressing adenovirus were generous gifts from H. Kurose (Kyushu University, Japan) and S. Hattori (Tokyo University, Japan), respectively.

Cell Culture and Transfection—Human umbilical vein endothelial cells (HUVECs) and human aortic endothelial cells (HAECs) were purchased from Cascade Biologics, Inc. (Portland, OR) and cultured in Humedia-EG2 as previously reported (24). HEK293T cells were generous gifts from Dr. B. J. Mayer (University of Connecticut) and maintained as described previously. Jurkat cells and HEK293 cells were obtained from the American Type Culture Collection (Manassas, VA) and cultured in RPMI 1640 (Invitrogen) and Dulbecco's modified Eagle's medium supplemented with 10% fetal bovine serum. Cultured cells were transfected using Lipofectamine 2000 reagent (Invitrogen).

Reverse Transcription-PCR, Pull-down Assay, Immunoprecipitation, and Immunoblotting—RNAs from cultured Jurkat cells and HUVECs were prepared by TRIzol (Invitrogen). cDNAs was synthesized by reverse transcriptase reaction using random primer and RNAs as templates. The cDNA specific for human RAPL was amplified by PCR using a primer set (5′RAPL, CTGGACGAGGAACTGGAAGACTGCTTC; 3′RAPL, AGGGATGGAGAAGGCATCCCACTCTAC). GTP-bound Rap1 was detected according to the method of Bos and co-workers (25). Briefly, HUVECs stimulated with 1 μM S1P for the time indicated at the *top* of Fig. 5 were lysed in lysis buffer (50 mM Tris, pH 7.5, 150 mM NaCl, 5 mM $MgCl_2$, 1% Nonidet P-40, 0.1% SDS, 0.5% deoxycholic acid, 1 mM Na_3VO_4). Precleared lysates were incubated with GST-Rap1-binding domain of RalGDS and glutathione-Sepharose beads. Proteins collected on the beads were subjected to SDS-PAGE followed by immunoblotting with anti-Rap1 antibody. Immunoprecipitation and immunoblotting were performed as described previously (26). Briefly, HEK293T transfected with plasmids as indicated in Fig. 1 were lysed using lysis buffer. Lysates were precleared by centrifugation at 15,000 × *g* for 10 min, followed by immunoprecipitation using anti-GFP and Protein A-Sepharose. Immunoprecipitates were subjected to SDS-PAGE and immunoblotting with anti-FLAG antibody and peroxidase-conjugated goat anti-mouse IgG as a primary and a secondary antibody, respectively. Proteins reacting with anti-FLAG were visualized by an ECL system (Amersham Biosciences) and an LAS-1000 system (Fuji Film, Japan).

Microtubule Binding Assay—Microtubule-associating protein-containing microtubule prepared from bovine brain were gifts from N. Yamagishi (Kyoto Pharmaceutical University, Japan). Glutathione *S*-transferase-fused RAPL (GST-RAPL) expressed in BL21-Star bacteria (Invitrogen) was collected on glutathione-Sepharose (Amersham Biosciences). GST-RAPL was eluted using 10 mM glutathione, precleared by centrifugation at 400,000 × *g*, and polymerized in microtubule-binding buffer (100 mM MES-KOH (pH 6.8), 2 mM EDTA, 1 mM $MgCl_2$, 10 mM Taxol, 4 M glycerol, and 1 mM GTP). For the microtubule binding assay, 5 μg of purified microtubules and GST-RAPL at the concentration indicated in Fig. 3 legend were mixed in 200 μl of microtubule-binding buffer for 30 min at 37 °C. After centrifugation at 400,000 × *g* for 15 min, equal amounts of the supernatant and the pellet were analyzed by SDS-PAGE and immunoblotting with anti-GST. Bovine serum albumin fraction V was used as a negative control for GST-RAPL.

Wound Healing Assay and Responses to Chemoattractant from a Micropipette—HUVECs or HAECs transfected with plasmids indicated in the figures were cultured on 35-mm glass bottom dishes coated with collagen until they reached the monolayer state. The cells were scratched by a regular 20-μl pipette tip along the diameter of the bottom glass. The culture medium remained unchanged during wound healing. Monolayer-cultured HUVECs infected with an adenovirus expressing rap1GAPII, an adenovirus expressing EGFP-RAPL, or an adenovirus expressing the RA mutant of RAPL were scratched and time lapse-imaged. HAECs expressing EGFP-RAPL or those expressing Raichu-Rap1 cultured on glass-bottom dishes coated with collagen were exposed to 1 μM S1P supplied by a micropipette (FemtoJet; Eppendorf Japan).

Fluorescence Microscopy and Confocal Imaging—HUVECs or HAECs transfected with plasmids expressing fluorescence-tagged proteins as indicated in the figure legends were imaged on an Olympus IX-81 inverted microscope. The microscope with a 75-watt xenon arc lamp was equipped with a cooled charge-coupled device camera, CoolSNAP-HQ (Roper Scientific), and two filter exchangers, controlled by MetaMorph 5.0 software (Molecular Devices). The EGFP image and DsRed image were obtained through an XF2043 dichroic filter (Omega) and either a set of an S484/15 excitation filter and an S515/30 emission filter or a set of an S555/25 excitation filter and an S630/60 emission filter, respectively, as reported previously (27). HUVECs transfected with pCA-EGFP-RAPL cultured on a collagen-coated glass-base dish were fixed by 4% paraformaldehyde at room temperature, followed by permeabilization with 0.1% Triton X-100. Permeabilized cells were incubated with anti-β-tubulin or anti-γ-tubulin antibody. Immunopositive reaction was visualized with Alexa 546 goat-anti-mouse IgG (Molecular Probes, Inc., Eugene, OR). Confocal images of EGFP and Alexa 546 were obtained by an Olympus BX50WI microscope controlled by Fluoview. To monitor the cell shape and localization of fluorescence-tagged molecules in living cells, a phase-contrast image and a fluo-